Dissertation
submitted to the
Combined Faculties for the Natural Sciences and for Mathematics
of the Ruperto-Carola University of Heidelberg, Germany
for the degree of
Doctor of Natural Sciences

Presented by
Diplom-Physicist Simone Astori
born in Pavia, Italy

Oral examination: 22.11.2006

Modulation of GABAergic transmission in the cerebellar stellate cell network by neurotransmitter spillover and synaptic cross talk

Referees: PD Dr. Georg Köhr

Prof. Dr. Josef Bille

ZUSAMMENFASSUNG

Modulation der GABAergen Übertragung im Netzwerk der zerebellären Sternzellen durch Neurotransmitter Spillover und synaptischen Cross Talk

Zerebelläre Sternzellen sind miteinander verknüpfte Interneurone in der äußeren Molekularschicht, die die Purkinje Zellen inhibieren und dabei den finalen Output vom Kleinhirn modulieren. In der vorliegenden Arbeit wurde das Netzwerk von Sternzellen mittels elektrophysiologischer Methoden auf der Ebene einzelner Synapsen untersucht. Es konnte gezeigt werden, dass erhöhter erregender Input in der Molekularschicht zur Depression der chemischen Übertragung zwischen Sternzellen führt. Diese Depression ist zurückzuführen auf eine Reduktion in der Freisetzungswahrscheinlichkeit des inhibitorischen Neurotransmitters γ-Aminobuttersäure (GABA). Die Analyse der synaptischen Parameter kombiniert mit der Anwendung von Pharmaka zeigte die Beteiligung metabotropischer $GABA_B$- Rezeptoren und ionotropischer L-α-Amino-3-hydroxy-5-methyl-4-isoxazol-propionsäure (AMPA)-Rezeptoren, die im Axon der Sternzellen lokalisiert sind. Ca^{2+}-Imaging Experimente mit Hilfe der Zwei-Photonen Mikroskopie bestätigten die Rolle von präsynaptischen Rezeptoren bei der Modulation axonaler Ca^{2+} Signale, die die GABA Freisetzung auslösen.

Diese Ergebnisse unterstützen die Relevanz von präsynaptischen Rezeptoren und erbringen neue Hinweise für Neurotransmitter Spillover und Cross Talk zwischen Synapsen und erweitern damit das Szenario der Signalübertragung in zentralen Synapsen.

SUMMARY

Modulation of GABAergic transmission in the cerebellar stellate cell network by neurotransmitter spillover and synaptic cross talk

Cerebellar stellate cells are interconnected interneurons located in the outer molecular layer. They provide inhibition to Purkinje cells, thereby modulating the final output of the cerebellum. In this work, electrophysiological means were employed to study the stellate cell network at the single synapse level. Sustained excitatory input invading the molecular layer was found to depress the chemical transmission between stellate cells, due to a decrease in the release probability of the inhibitory neurotransmitter γ-Aminobutyric acid (GABA). Analysis of synaptic parameters combined with the application of pharmacological tools indicated the involvement of metabotropic $GABA_B$ receptors and ionotropic L-α-amino-3-hydroxy-5-methyl-4-isoxazolepropionic acid (AMPA)-receptors localized in the axon of stellate cells. Ca^{2+} imaging experiments performed with Two-photon Microscopy confirmed the role of presynaptic receptors in affecting the axonal Ca^{2+} signals that trigger GABA release.

These findings support the relevance of presynaptic receptors and provide another example of neurotransmitter spillover and cross talk between synapses, enriching the scenario of signal transmission at central synapses.

Content

1. INTRODUCTION

1.1 Signal transmission in the central nervous system

The nervous system consists of individual nerve cells called neurons and neuro glial cells. The human brain contains 10^{11} neurons and 10 times as many glial cells. Whereas neurons are generally perceived to be the major cells to process information, glial cells are thought to provide the brain with structure, sometimes insulate neuronal groups and synaptic connections from each other. Certain classes of glial cells guide migrating neurons and direct the outgrowth of axons. Furthermore, glial cells help to form the blood-brain barrier, remove cellular debris and secrete trophic factors. Glial cells might also be involved in long range signaling, coordinating activity in different parts of the brain (Fields and Stevens-Graham, 2002).

Nevertheless neurons are the electrical excitable cells, which process and exchange signals with one another. The anatomy and distinct cellular shape of neurons were first described by Ramón y Cajal by staining neuronal tissue with the Golgi staining method (Cajal, 1894).

1.1.1 Nerve cells: morphology and types

Neurons are classically divided into two functional classes: *principal* (or *projection*) *neurons* and *interneurons*. Principal neurons convey information to the next stage of the functional system in the brain. In contrast, interneurons contact only local cells involved in the same processing state, thereby often inhibiting their target neurons.

Although neurons differ from one another, depending on location and function, they all share features that distinguish them from the cells in other tissues (Fig. 1.1). In addition to the *cell body* (*soma*), which contains the nucleus and the organelles for homeostasis and protein synthesis, neurons possess specialized input and output regions. The regions where neurons receive input from other neurons are the dendrites. Dendrites are characterized by a highly branching, treelike shape. Little protrusions from the *dendrite* are called spines. These are amongst others the structures that form the points of contact, called *synapses*, to other cells. The output region of a neuron is the *axon*. It also shows extensive branching. The structures contacting other neurons, mainly on spines and dendritic shafts, are the so-called *boutons*. In many types of neurons boutons appear as an ‘en passant’ thickening of the axonal cable.

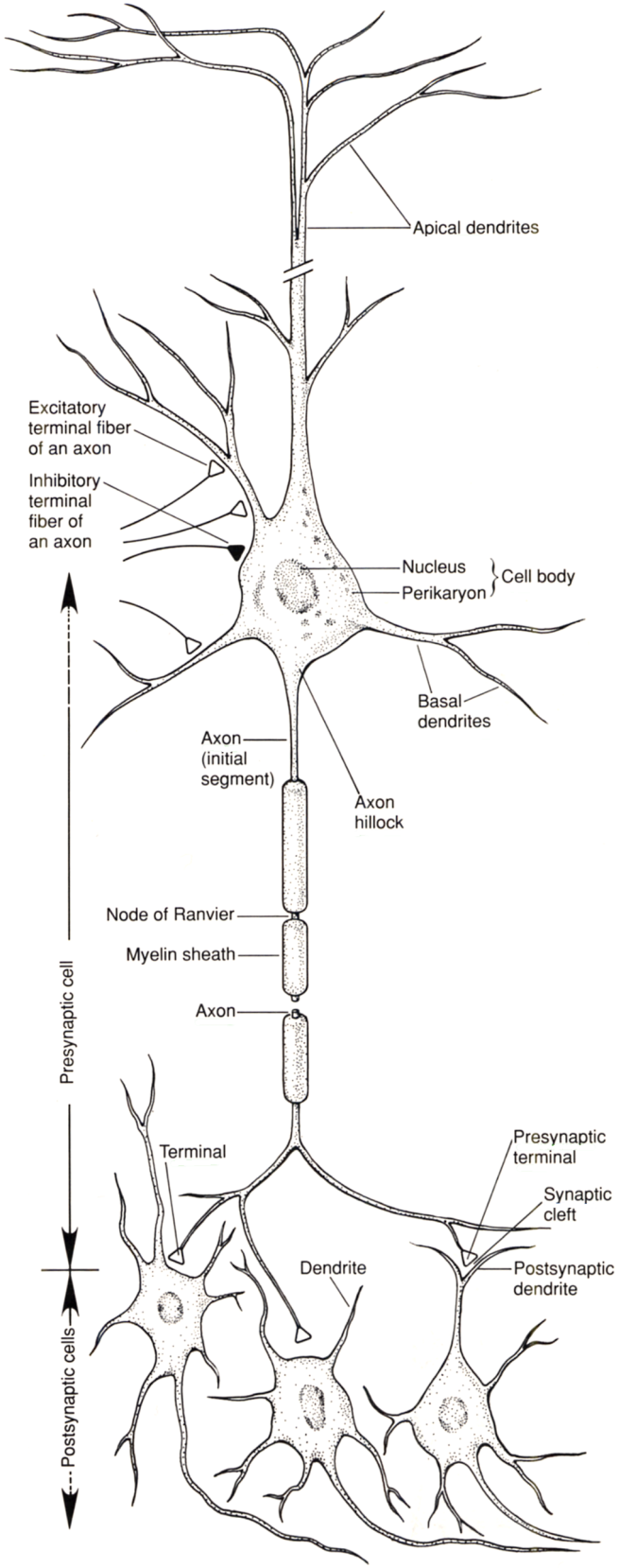

Figure 1.1 ***Morphological features of nerve cells***
The cell body (soma) contains nucleus and perikarion, and gives rise to two types of processes: dendrites (both apical and basal) and axons. The axon is the transmitting element of the neuron. Axons vary greatly in length, with some extending more than 1 meter. The axon hillock, the region of the cell body where the axon emerges, is where the action potential is initiated. Many axons are insulated by a fatty myelin sheath, which is interrupted at regular intervals by regions known as nodes of Ranvier. Branches of the axon of one neuron (the presynaptic neuron) form synaptic connections with the dendrites or cell bodies of another neuron (the postsynaptic cell). The branches of the axon may form synapses with as many as 1000 another neurons. (Adapted from Kandel's textbook)

1.1.2 Resting membrane potential

The membrane of all cells, including nerve cells, is about 6-8 nm thick and consists of a mosaic of lipids and proteins. The surface of the membrane is formed by a double layer of lipids in which various membrane proteins are embedded. Besides structural proteins, these are enzymes, receptors, pumps and channels. The combination of special kinds of receptors, pumps and channels enables nerve cells to transmit and receive electrical signals, a feature that other cells do not show. Ion pumps and ion channels make the cell membrane permeable to charged ions. By means of metabolic energy, mainly in the form of hydrolyzing ATP, ion pumps generate an ion gradient across the membrane against the electrochemical gradient.
The different distribution of charges across a semipermeable membrane gives rise to a potential difference across the membrane. At steady-state equilibrium the resting membrane potential V_m is given by the Goldman-Hodgkin-Katz equation

$$V_m = \frac{RT}{F} \ln \frac{\sum_k z_k P_k [X_k]_o + \sum_l z_l P_l [Y_l]_i}{\sum_k z_k P_k [X_k]_i + \sum_l z_l P_l [Y_l]_o}$$

for different positively charged ionic species X and different negatively charged ionic species Y, with their respective valences z and total permeabilities P on the outside (o) and inside (i) respectively. R is the gas constant (R = 8.31 $Jmol^{-1}K^{-1}$), T the absolute temperature and F the Faraday constant (F = 96485.31 $Cmol^{-1}$). The ion channels of neurons make the membrane mainly permeable to potassium, sodium, chloride and calcium ions, thus the resting membrane potential can be calculated taking only these ion species into account (Table A). The resting membrane potential ranges typically from –80 mV to –60 mV depending on the cell type.

Ion	$[x_i]$ (mM)	$[x_o]$ (mM)
Na^+	10	121.25
K^+	145	2.5
Ca^{2+}	0.000046	2
Cl^-	20	133.5

Table A ***Ionic concentrations***
Concentrations of the main ion species responsible for the resting membrane potential inside of the cell [x_i] and in the extracellular space [x_o].

1.1.3 Action potentials

The most important feature for signal transmission of nerve cells is their capability to actively transfer information by generating an output signal called action potential. The action potential is an all-or-none, stereotyped, transient depolarizing electrical signal, which spreads along the axon actively without attenuation (Fig. 1.2). The mechanism underlying generation and propagation of action potentials is the interplay of voltage sensitive sodium and potassium channels (Fig. 1.3). Above a certain membrane potential threshold (typically –40 mV), which is reached upon depolarizing postsynaptic signals terminating on the neuron, voltage sensitive sodium channels have a higher probability to be in the open configuration (i.e. the channel opens). This results in a further depolarization, since the membrane potential is driven towards the equilibrium potential for sodium (around +50 mV). Neighbouring stretches of membrane, which also contain voltage dependent sodium channels, are subsequently equally depolarized resulting in a spread of the excitation along the membrane. By way of this regenerative self-amplifying process, most of the sodium channels can switch to their open state in less than 1 ms. Then the voltage sensitive sodium channels rapidly inactivate, thereby reducing the sodium permeability of the membrane. Voltage gated potassium channels, which have opened during the depolarization, lead to a potassium influx into the cell and cause a rapid hyperpolarization of the membrane back to the resting potential.

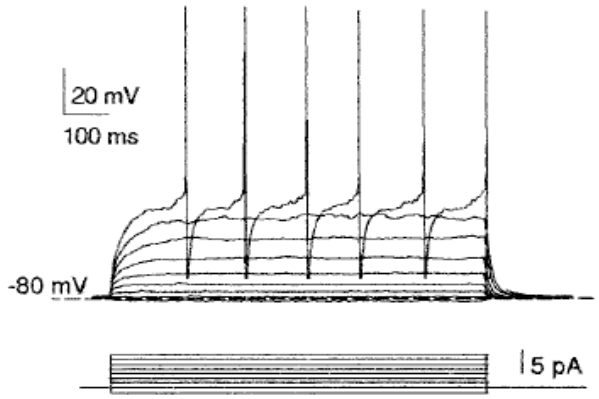

Figure 1.2 ***Action potentials***

When a nerve cell is depolarized above a certain threshold (typically –40 mV) action potentials are generated. In this case the depolarization was provided by current injections into the soma in a current-clamp experiment.
Action potentials are all-or-none events having same shape and amplitude, which are characteristic for each cell type, as is the firing frequency.

The process of action potential generation can be explained by looking at the current *I* across the cell membrane for a given ion species X with a conductance of *g*, which is given by

$$I_x = g_x (V_m - V_{rev})$$

where V_m is the membrane potential and V_{rev} is the reversal potential for the ion species. The conductance g_x is voltage dependent and can be described for the different ion channels and their different kinetic properties by the Hodgkin-Huxley equation, a system of differential equations for the rate constants of channel opening, closing and inactivation (Hodgkin and Huxley, 1952).

The axon initial segment close to the soma, also called the axon hillock, has a high density of voltage sensitive sodium channels. In this region the incoming excitatory and inhibitory postsynaptic potentials are 'integrated' and 'compared' to the threshold value (determined by the channel density) of action potential firing, i.e. if a certain depolarization is reached, an action potential is initiated. The action potential is then transmitted along the axon actively in an all-or-none fashion and with a stereotyped shape.

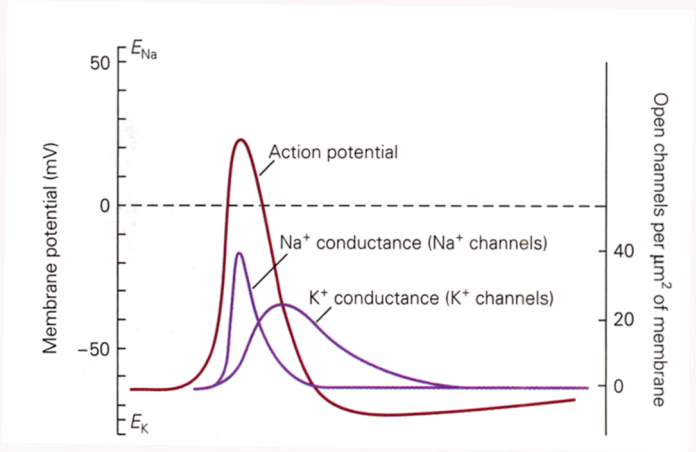

Figure 1.3 ***Generation of action potentials***

The shape of the action potential can be calculated from the changes in g_{Na} and g_K that result from the opening and closing of voltage gated Na^+ and K^+ channels. The Na^+ current and the K^+ current are responsible for the depolarizing and hyperpolarizing phase of the action potential, respectively. (Adapted from Kandel's textbook)

1.1.4 Synapses

Information is transferred between neurons by two types of synaptic transmission: electrical and chemical. Electrical transmission is mediated by the direct flow of current from the presynaptic to the postsynaptic neuron through gap junctions, which are established through protein pores connecting the two membranes. The pore forming transmembrane proteins

linking the lumen of both cells across the extracellular space are connexins. The connexin composition of the gap junction results in rectifying or nonrectifying electrical connections of different conductances. Electrical signaling via gap junctions is fast, without latency and it can result in the synchronization of the coupled neurons. Graded, subthreshold deviations from the resting membrane potential can be equally transmitted. Gap junction coupling is development dependent and seems to decrease with age (Bennett et al., 1997).

Chemical synaptic transmission is slower than electrical transmission because the presynaptic neuron must first release a neurotransmitter, which then diffuses across the synaptic cleft and binds to receptors in the postsynaptic cell membrane. Nevertheless, chemical synapses are more numerous and play a major role, since they can undergo plastic changes.

Chemical synapses are specialized structures, where the membrane of the presynaptic neuron is close to the postsynaptic membrane, being just separated by the synaptic cleft. At the point of contact, both membranes contain a high density of proteins for signal transduction (Husi et al., 2000). The sum of all single synaptic contacts existing between two neurons is referred to by the term synapse, coined by Sherrington. The distributed strength of all synapses has been proposed to be the basis of memory traces.

1.1.5 Chemical synaptic transmission

The anatomical basis of the synaptic contact is the presynaptic density located in a bouton or terminal in close vicinity to the postsynaptic density, mainly located on a spine head or a dendritic shaft. Pre- and postsynaptic membranes are spatially separated (and thus electrically isolated) by a 10 nm gap, the synaptic cleft. The presynaptic active zone is characterized by a cluster of vesicles containing neurotransmitter close to the membrane and a high density of voltage sensitive Ca^{2+} channels (Fig. 1.4).

Upon invasion of the axonal tree by an action potential, the voltage sensitive Ca^{2+} channels open. This results in Ca^{2+} influx into the presynaptic terminal. Ca^{2+} binds to proteins that trigger the fusion of the vesicles with the plasma membrane. Subsequently, a fusion pore opens, expands and leads to the release of neurotransmitter from the lumen of the vesicle into the synaptic cleft. This mechanism of neurotransmitter release is called exocytosis, a highly regulated process of multiple protein-protein interactions for which influx and binding of Ca^{2+} is a prerequisite. The vesicle membrane is recovered from the plasma membrane again by endocytosis and the vesicles are either recycled and reloaded with neurotransmitter or

degraded. The neurotransmitter diffuses across the synaptic cleft and binds to receptors on the postsynaptic membrane.

In the CNS, synaptic transmission can either be excitatory or inhibitory. The main excitatory transmitter in the brain is glutamate, which acts on three different types of ionotropic receptors termed α-amino-3-hydroxy-5-methyl-4-isoxazolepropionic acid (AMPA), kainate and N-methyl-D-aspartate (NMDA) receptors and on metabotropic G-protein coupled glutamate receptors (mGluRs). The main inhibitory transmitters in the CNS are γ-Aminobutyric acid (GABA) and glycine. GABA receptors are divided into ionotropic $GABA_A$ receptors and metabotropic G-protein coupled $GABA_B$ receptors.

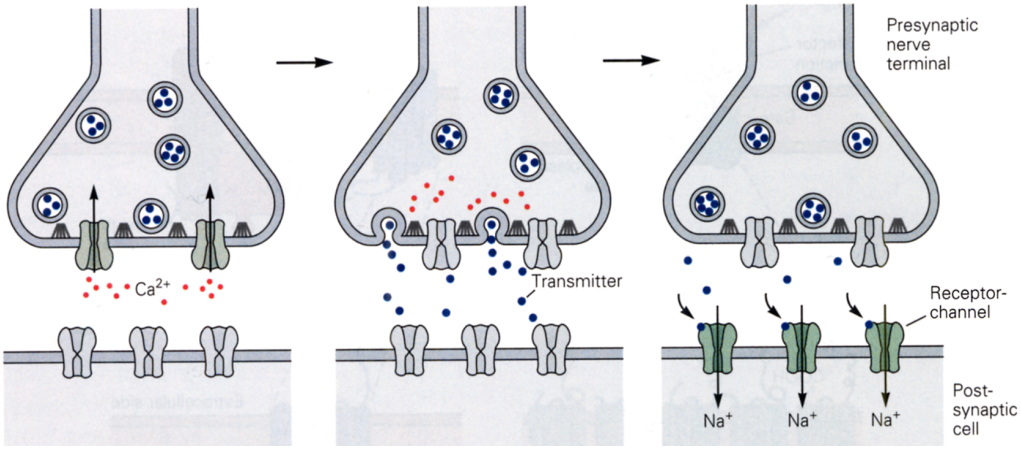

Figure 1.4 ***Neurotransmission at chemical synapses***

Depolarization of the axon terminal by action potentials triggers Ca^{2+} influx through voltage gated Ca^{2+} channels. This leads to fusion of the vesicles into the cell membrane and liberation of neurotransmitter, which then diffuses in the synaptic cleft and binds to postsynaptic receptors. Gating of postsynaptic receptors (in this case AMPARs) generates flux of Na^+ ions and consequent depolarization of the postsynaptic cell. (Adapted from Kandel'tetxbook)

1.1.6 Glutamate receptors

Ionotropic glutamate receptors (iGluRs) are ligand-gated channels, which are selectively permeable for cations, principally Na^+, K^+ and sometimes Ca^{2+} ions. On the basis of their responsiveness to certain glutamate derivatives, iGluRs are classified into AMPA, NMDA and kainate receptors.

The fast excitatory neurotransmission at most synapses in the CNS is mediated by AMPARs, defined by their sensitivity to the glutamate analogue α-amino-3-hydroxy-5-methyl-isoxazole-4-propionic acid (AMPA). This group of glutamate receptors form cationic ion

channels, which after binding of glutamate are mainly permeable to Na^+ and K^+ ions. Opening of these channels at the resting membrane potential leads to a rapid depolarization of the postsynaptic membrane. The cationic depolarizing current flowing through AMPARs can be measured in voltage-clamp condition as EPSC (Excitatory PostSynaptic Current).

The second type of glutamate receptor is the N-methyl-D-aspartate (NMDA) receptor channel. The prevailing conductance state of the NMDA receptor is determined not only by binding of glutamate, but also by the membrane potential. At resting membrane potential the ion channel pore is blocked by Mg^{2+}. In this state, binding of glutamate only makes the receptor channel permeable to a small extent, and then only to Na^+ and K^+ ions. If the membrane is depolarized more strongly the Mg^{2+} is removed. So, if binding of glutamate to the NMDA receptor is accompanied by membrane depolarization to relieve the Mg^{2+} block, the receptor channel also becomes permeable to Ca^{2+}. Thus, the NMDA receptor channel needs two events occurring at the same time to become activated. This property of the NMDA receptor is assumed to be the underlying mechanism for coincidence detection during pre- and postsynaptic activity (Yuste et al., 1995; Koester et al., 1998), which might be important to induce activity dependent changes in synaptic strength on the single synaptic contact level.

Another class of glutamate receptors are the metabotropic glutamate receptors (mGluRs). These are membrane spanning receptor proteins which trigger biochemical reactions mainly through G-protein coupled signaling cascades.

While ionotropic receptors mediate fast synaptic action in the millisecond range, metabotropic receptors mediate synaptic actions in the second-to-minute range, often associated with changes in neuronal excitability and synaptic strength. Furthermore, while glutamate always has an excitatory effect on iGluRs, mGluRs can produce either excitation or inhibition.

1.1.7 GABA receptors

The main inhibitory neurotransmitter in the brain is γ-Aminobutyric acid (GABA). The associated ligand-gated channels are $GABA_A$ receptors ($GABA_A$Rs), which are permeable to Cl^- and bicarbonate anions. Opening of these channels at the resting membrane potential leads to a rapid hyperpolarization of the postsynaptic membrane. The ionic hyperpolarizing current flowing through $GABA_A$Rs can be measured in voltage-clamp condition as IPSC (Inhibitory PostSynaptic Current). The inhibitory action of GABAergic transmission depends on the

intracellular concentration of Cl^-. In some conditions, e.g. in early developmental stages, activation of $GABA_A$Rs may lead to excitation (see below).

GABA may also initiate a metabotropic pathway by activating metabotropic $GABA_B$ receptors. These members of the GABA receptor family couple to $G_{i/o}$ proteins and can either block Ca^{2+} channels or activate K^+ channels (Misgeld et al., 1995). The Ca^{2+} blocking type appears to act presynaptically, whereas the receptor that activates K^+ conductance can be found at postsynaptic sites (Yamada et al. 1999). As a functional consequence, activation of $GABA_B$ receptors at axon terminals causes presynaptic inhibition of the release of several neurotransmitter, including glutamate and GABA itself, whereas activation of somatodendritic $GABA_B$ receptors hyperpolarizes many types of neurons, leading to a decrease in firing rate (Misgeld et al., 1995).

1.1.8 Excitation and inhibition: the electrophysiological point of view

Gating of postsynaptic channels after binding of neurotransmitter generates an ion flux through the cell membrane that can be measured by electrophysiological means. The patch-clamp technique (see Methods) allows recording of either small changes in the membrane potential (current-clamp mode) or small currents flowing through the cell membrane (voltage-clamp mode). We will focus on this latter recording mode, which was used for our recordings.

In the case of transmission at glutamatergic synapses the resulting electrical postsynaptic signal is an Excitatory PostSynaptic Current (EPSC) determined by the conductance change after binding of glutamate to iGluRs.

For example, considering a neuron at resting membrane potential (typically -60/-70 mV), opening of AMPARs leads to a flux of Na^+ ions from the extracellular compartment into the cytoplasm and to a flux of K^+ in the opposite direction, according to the Nernst's equation for the two ion species. The resulting current is a flux of positive charge into the cell, conventionally measured as inward current, which depolarizes the cell.

In the case of transmission at GABAergic synapses the resulting electrical postsynaptic signal is an Inhibitory PostSynaptic Current (IPSC). When GABA binds to postsynaptic $GABA_A$ receptors, the negatively charged Cl^- ions (and to a less extent bicarbonate ions) are allowed to flow from the extracellular compartment into the cytoplasm, resulting in a net outward current that hyperpolarizes the cell.

The depolarizing and hyperpolarizing signals generated on the postsynaptic membrane at the different excitatory and inhibitory connections then spread passively along the dendritic tree. The shape, size and passive membrane properties of the dendrites determine the attenuation and filtering of the initial PSCs as they travel towards the soma and the axon initial segment (Bekkers et al, 1996; Hausser et al., 2001), where integration of all postsynaptic signals occurs.

Size and shape of a PSC at the postsynaptic membrane are determined by the number and time course of discrete neurotransmitter quanta released from the presynaptic terminal and by the postsynaptic channel density (Silver et al., 1996).

Synaptic transmission is not reliable. The release of a quantum (of neurotransmitter) of quantal size *q* from a presynaptic terminal occurs only with a certain probability *p*. According to the quantal hypothesis of synaptic transmission, the size of the postsynaptic currents measured at the soma should be binomially distributed (Castillo and Katz, 1954; Bekkers et al., 1994). Quantal analysis can yield *q*, *p* and the number of synaptic contacts *n* (Redman et al., 1990). Since the release probability and the quantal size can vary between single synaptic contacts, a clear cut binomial distribution of PSC amplitudes can not be measured at all synapses (Wahl et al., 1995).

A method for unravelling the quantal feature of chemical synaptic transmission is to record spontaneous synaptic activity in the presence of tetrodotoxin (TTX). This compound blocks the generation of action potentials by blocking voltage dependent Na^+ channels. In this way it is possible to record only the miniature events (*minis*) that arise from spontaneous transmitter release. These events depend on the fluctuation of the intracellular Ca^{2+} concentration at the presynaptic site, which can lead to the fusion of one or few vesicles into the presynaptic membrane. Miniature excitatory (mEPSCs) and inhibitory (mIPSCs) currents are characterized by different properties, in term of frequency and amplitude of the events, depending on the type of pre- and postsynaptic cell, but are always present as background of synaptic transmission and their analysis is useful to gain knowledge about presynaptic and postsynaptic function, such as release probability and number of synaptic contacts (from the mini frequency) or density of postsynaptic receptors (from the mini amplitude).

In electrophysiological recordings, the current signals measured in voltage-clamp mode can be classified into three categories, depending on the underlying type of synaptic release:

eEPSCs (eIPSCs) = evoked excitatory (inhibitory) postsynaptic currents, generated upon stimulation of presynaptic fibers to induce glutamate (GABA) release.

sEPSCs (sIPSCs) = spontaneous excitatory (inhibitory) postsynaptic currents, recorded without simulation of the afferent presynaptic fibers: the recorded events are generated by an ensemble of action potential dependent release, due to spontaneous firing of presynaptic cells, and action potential independent quantal release.
mEPSCs (mIPSCs) = miniature excitatory (inhibitory) postsynaptic currents, due to action potential independent quantal release (*minis*).
In the same way, the changes in membrane potential recorded in the current-clamp mode can be defined as:
eEPSPs (eIPSPs) = evoked excitatory (inhibitory) postsynaptic potentials.
sEPSPs (sIPSPs) = spontaneous excitatory (inhibitory) postsynaptic potentials.
mEPSPs (mIPSPs) = miniature excitatory (inhibitory) postsynaptic potentials.

1.1.9 Short term plasticity, long term plasticity and memory

Synaptic transmission also depends on the history, i.e. previous activity, of the synaptic contact. The capability to undergo plastic changes is a unique feature of chemical synapses. One usually refers to modifications that last for a short time window (milliseconds or some seconds) as short term plasticity, whereas changes lasting for hours or even days are considered as long term plasticity.
Activity dependent short term plasticity can result in facilitation or depression of synaptic transmission to a subsequent action potential (Thomson et al., 1993; Stevens and Wang, 1995; Markram and Tsodyks, 1996). Short term effects are mainly accounted for by presynaptic mechanisms (Katz and Miledi, 1968; Rahamimoff, 1968; Betz, 1970; Zucker, 1989). An action potential arriving at a terminal causes Ca^{2+} influx but not necessarily transmitter release. In the case of low release probability, the postsynaptic current can be absent (failure) or small, depending on the number of release sites. A second action potential arriving with a short delay might add additional Ca^{2+} ions to the residual Ca^{2+} from the first action potential, thus increasing the total amount of Ca^{2+} in the terminal. This higher concentration of Ca^{2+} might trigger release more reliably and can result in the release of more quanta giving rise to a larger postsynaptic current (*paired-pulse facilitation*). On the other hand, a high release probability implicates more release upon the first action potential, which might deplete the pool of readily releasable vesicles for a subsequent second action potential resulting in a smaller postsynaptic current (*paired-pulse depression*). The exact determinants of facilitation

and depression at a synapse are more complex, but it seems that the type of postsynaptic cell determines the direction of the short term plasticity effects (Reyes et al., 1998).

Long term modifications are induced by specific patterns of pre- and postsynaptic activity, which result in permanent changes of synaptic transmission properties. Since behaviour is reflected in a certain pattern of electrical activity, it makes sense to assume that experience dependent modifications of behavioural output are based on changes of the electrical excitability of the underlying neuronal circuits. Long term potentiation (LTP) and long term depression (LTD) are long lasting activity dependent changes in synaptic strength between neurons (Isaac et al., 1995; Nicoll and Malenka, 1995; Luscher et al., 2000; Malinow et al., 2000). These effects were first reported experimentally by Bliss and Lomo in the hippocampus (Bliss and Lomo, 1970). Since then LTP and LTD have been observed at many synapses in different brain regions. It is widely believed that these phenomena provide an important key to understand the cellular and molecular mechanisms by which memories are formed and stored (Bliss and Collingridge, 1993). Furthermore, they might underlie the development and refinement of neuronal networks (Crair and Malenka, 1995).

1.1.10 Spillover and Cross Talk

From the classical point of view, synapses work as private channels of communication, in which only directly apposed postsynaptic receptors detect the release of transmitter. Some intriguing studies, however, suggested that in different central synapses released transmitter molecules activate receptors located outside the synaptic cleft (Kullmann et al., 1996; Rossi and Hamann, 1998; Satake et al., 2000). Because transmitter molecules must diffuse out of the synaptic cleft for this type of activation to occur, researchers have termed this phenomenon *spillover*. Diffusing transmitter could potentially activate receptors located extrasynaptically, for example on presynaptic fibers, or even in neighboring synapses (Fig. 1.5). In the latter case, molecules released at one synapse would generate *cross talk* with nearby synapses, which would enrich the scenario of synaptic transmission.

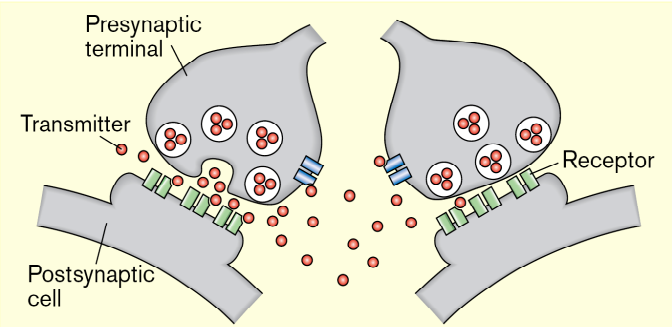

Figure 1.5 ***Transmitter spillover and cross talk between synapses.***
The synapse on the left releases neurotransmitter, activating postsynaptic receptors (green). Transmitter molecules that diffuse away from the synaptic cleft can activate presynaptic receptors (blue) and postsynaptic receptors of a nearby synapse (from Huang, 1998).

1.2 The cerebellum

The cerebellum constitutes only 10% of the total volume of the brain, yet it contains more than half of all neurons. It is involved in motor coordination, posture and balance: a lesion of the cerebellum can disrupt coordination of the limb and eye movements, impair balance and decrease muscle tone. The cerebellum plays also a role in motor learning, is involved in calibration and adaptive adjustments of motor programs, and may also contribute in perception.

The cerebellum works as a comparator that compensates for errors in movements by comparing intention with performance. It receives inputs from the brain regions that are involved in programming and execution of movement (*corollary discharge* or *internal feedback*) and information from the periphery about the actual movement (*reafference* or *external feedback*). It then compares internal with external feedback and corrects the errors by sending its output to the descending motor system of the brain.

The cerebellum is organized into three functional regions, each with distinct anatomical connection to the brain and spinal cord: the vestibulocerebellum, the spinocerebellum and the cerebrocerebellum. The vestibulocerebellum controls balance and eye movements; the spinocerebellum adjusts ongoing movements; the cerebrocerebellum coordinates the planning of limb movements. A schematic drawing of the functional components and their outputs is shown in Fig. 1.6.

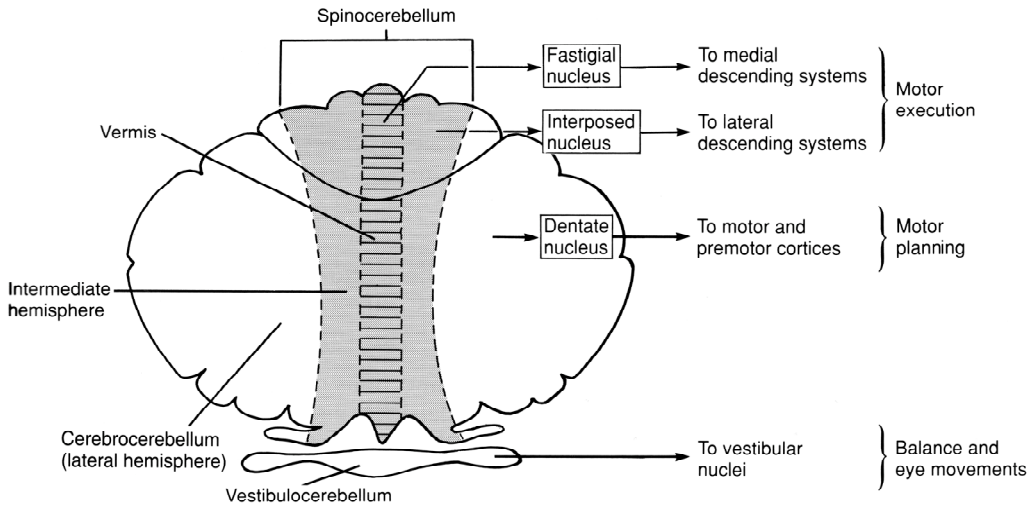

Figure 1.6 ***Cerebellar functional components***

Schematic drawing of cerebellar functional components with their outputs (adapted from Kandel's textbook).

The cerebellar cortex is a simple structure consisting of three layers that contain five types of neurons: stellate cells and basket cells, Purkinje cells, granule cells and Golgi cells (Fig. 1.7).

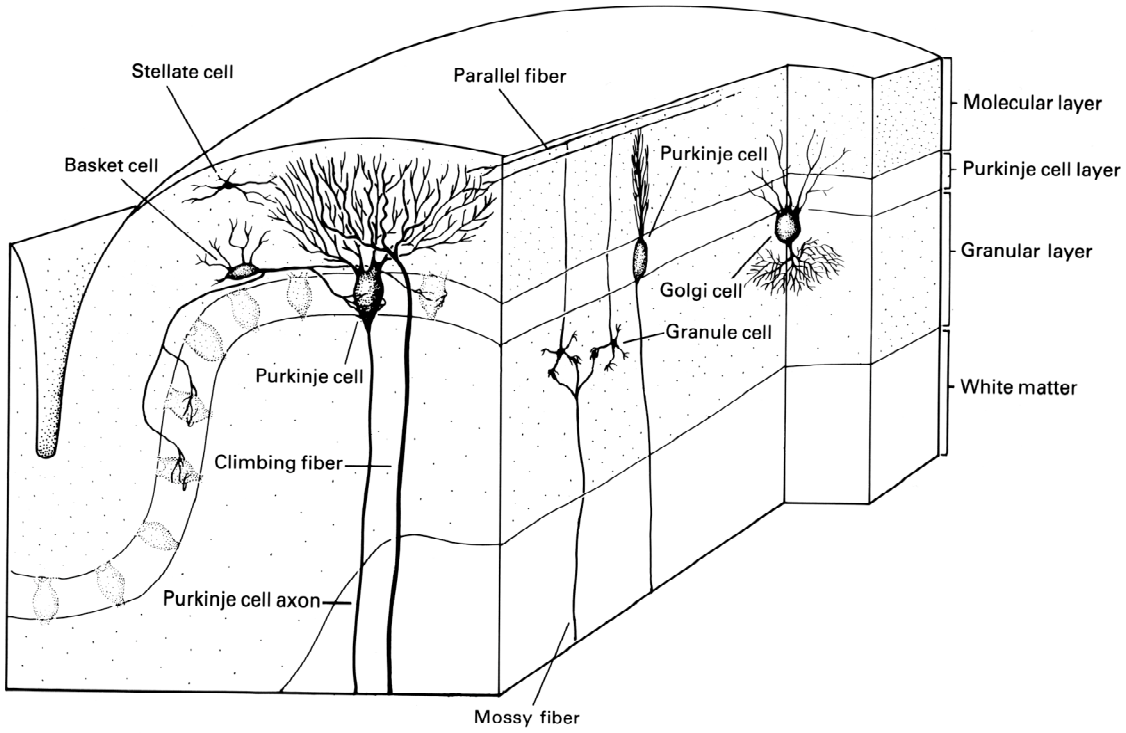

Figure 1.7 ***Cerebellar cortex***

Vertical section of a single cerebellar folium, in both sagittal and transverse planes, illustrating the general organization of the cerebellar cortex and the different types of cerebellar neurons (adapted from Kandel's textbook).

The principal neurons, i.e. the cells projecting their output out of the cerebellum, are the *Purkinje cells*. Unlike other principal neurons in the CNS, they are inhibitory and use GABA as neurotransmitter. They have large cells bodies (50-80 μm) and are arranged side by side in a single layer. The Purkinje cells have extensive dendritic trees that extend up into the molecular layer in a single sagittal plane. They receive excitatory input from two pathways:

1. the *climbing fibers*, which originate in a single site in the medulla, the inferior olivary nucleus, run through the granular layer and innervate the soma and the dendrites of the Purkinje cells making numerous synaptic contacts. Each climbing fiber contacts only 1-10 Purkinje cells, and each Purkinje cell receives synaptic inputs from only a single climbing fiber.
2. the *granule cells*, which are small compact neurons densely packed in the granular layer. Their number, about 10^{11}, exceeds the total in the cerebral cortex. They receive excitation from the *mossy fibers* (which originate from a variety of brain stem nuclei

and from neurons in the spinal cord that give rise to the spinocerebellar tracts) and inhibition from the *Golgi cells*, located in the granular layer. The axons of the granule cells project into the molecular layer and bifurcate into the *parallel fibers*, which run perpendicular to the sagittal plane. Each Purkinje cell receives approximately 200.000 inputs from parallel fibers.

The interneurons of the molecular layer modulate these two excitatory pathways by sending their GABAergic inhibitory output to the Purkinje cells.

The *basket cells* are located near to the Purkinje layer and contact the soma of Purkinje cells with a huge basket-shaped synaptic terminal.

The *stellate cells* are located in the outer molecular layer and innervate the dendrites of Purkinje cells and interneurons.

1.2.1 Cerebellar stellate cells

Stellate cells, together with the closely related basket cells, constitute the two classically distinguished types of inhibitory interneurons in the molecular layer of the cerebellar cortex. Stellate cell somata are located in the external two-thirds of the molecular layer, while basket cell somata are in the internal third, proximal to Purkinje cell bodies. Besides the morphological differences, the separation of the cerebellar interneurons in two distinct classes is substantiated by the fact that stellate cells occur in the cerebella of all classes of vertebrates that have been examined, whereas basket cells appear only in birds and mammals.

Stellate cells have dendritic and axonal arborization that are essentially contained in a single plane which is parallel to the sagittal plane for the part of the cerebellum close to the centre of the vermis. Their axons tend to run parallel to the Purkinje cell layer in the sagittal direction (Fig. 1.8). Stellate cells receive excitatory inputs mainly from parallel fibers (but also from climbing fibers) and send their inhibitory synapses to Purkinje cells and to other interneurons (Palay and Chan-Palay, 1974). Moreover stellate cells communicate with each other via electrical gap junctions (Galarreta and Hestrin, 2001). Stellate cells fire action potentials even in the absence of synaptic input (Llano and Gerschenfeld, 1993; Llano and Marty, 1995). Their voltage-dependent conductance mechanisms have been studied in detail (Midtgaard, 1992).

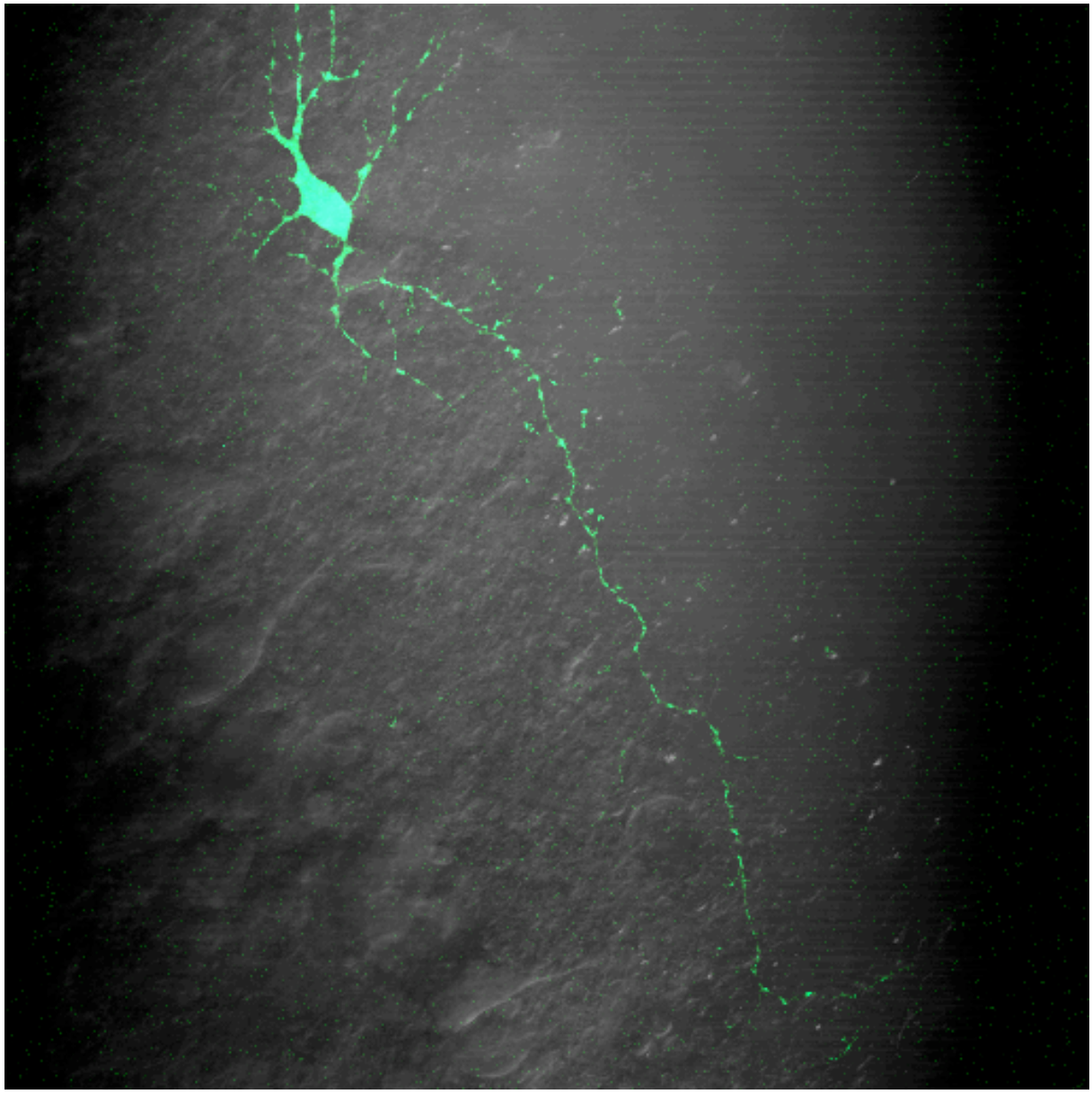

Figure 1.8 ***Morphology of stellate cells***

Dendritic branches extend from the cell body in every direction, whereas the thinner axon elongates in the sagittal direction parallel to the Purkinje cell layer. Somata of Purkinje cells and granule cells are visible in the lower left part of the image. The stellate cell was loaded with the Ca^{2+} *indicator Oregon Green 488 BAPTA-1 via the patch pipette (which was retracted after filling) and imaged with Two-photon microscopy. This picture is a z-projection elaborated by collecting the maximum intensity from 45 images taken in different focal planes with 1 µm intervals. Acquisition channels for infrared light and green fluorescence were overlaid. Image size: 206.8 µm x 206.8 µm.*

1.2.2 Glutamatergic transmission in stellate cells

As in most glutamatergic synapses in the CNS, the fast excitatory neurotransmission in stellate cells is mediated by AMPARs (Barbour et al., 1994). Glutamate liberated by action potential independent quantal release, action potential dependent spontaneous release or evoked by a single stimulus of the presynaptic parallel fibers generates respectively mEPSCs, sEPSCs and eEPSCs in the postsynaptic stellate cell that can be blocked by specific AMPAR blocker. These three types of release produce in the synaptic cleft a brief transient of glutamate which is rapidly removed by diffusion and glutamate transporters. In contrast, a train of stimuli can produce much more glutamate release because of presynaptic facilitation and delayed release (Atluri and Regehr, 1996, 1998). The resulting glutamate levels may be sufficiently large to overwhelm clearance mechanisms, allowing an extended glutamate signal and even glutamate spillover to nearby sites. It has been shown that this type of release plays a pivotal role in the excitatory transmission in stellate cells, since the NMDARs are rather expressed extrasynaptically in these interneurons. Brief stimulus trains at high frequency (e.g. 5 stimuli at 100 Hz) delivered to the parallel fibers can induce a spillover of glutamate which can escape the synaptic cleft and activate the perisynaptic NMDARs in interneurons (Carter and Regehr, 2000; Clark and Cull-Candy, 2002). This facilitated release resembles in vivo conditions, since granule cells are able to fire bursts of action potentials upon whisker deflection (Chadderton et al., 2004). This spiking pattern is directly linked to induction of plasticity at parallel fiber-to-interneuron synapses, since it can initiate a form of NMDAR dependent LTP (Smith and Otis, 2005). Another recent study reports that repetitive stimulation at the same synapse induces LTD and requires opening of Ca^{2+} permeable AMPARs and signaling through mGluR1 and cannabinoids receptors (Soler-Llavina and Sabatini, 2006).

1.2.3 GABAergic transmission in stellate cells

Stellate cells receive GABAergic inputs from other stellate cells. Recent findings indicate also the presence of autoreceptor currents (Pouzat and Marty, 1999), i.e. the axon projecting from a stellate cell may also contact the cell itself.

Miniature IPSCs recorded in the presence of TTX have mean amplitudes as large as those of spontaneous TTX-sensitive IPSCs (Llano and Gerschenfeld, 1993). This indicates that stellate-stellate synapses include only a few release sites with a large quantal size. Further

studies (Kondo and Marty, 1998) have classified the connections between stellate cells into simple connections involving a single functional release site (peak amplitude of GABAergic currents are described by a single Gaussian) and into complex connections, arising from the combination of two or three components (giving rise to multiple Gaussian curves), where each element behaves as a simple connection.
In sagittal cerebellar slices from mice or rats the level of connectivity among stellate cells is relatively high compared with values reported in other brain regions. The mean number of presynaptic cells contacting a stellate cell has been estimated as 4.25 (Kondo and Marty, 1998).

1.2.4 Coexistence of excitatory and inhibitory GABAergic transmission in cerebellar interneurons

Functional GABA synapses are usually assumed to be inhibitory. In mammals, postsynaptic effects of GABAergic synapses primarily result from the transient opening of $GABA_A$ channels, which are mainly permeant for Cl^-. The net ion flux through GABA channels is governed by the Nernst's equation and results from the sum of electrical and chemical gradients that are generated across the cell membrane.
During embryonic life, neurons accumulate Cl^-, probably through the Na^+-K^+-Cl^- cotransporter (NKCC1; Vardi et al., 2000). Since the intracellular concentration of Cl^- is high, activation of GABA receptors produces an outflow of negativly charged Cl^- ions, which corresponds to an inward current that depolarizes the cell. In this sense, GABAergic transmission is excitatory in early developmental stages. In later stages, when the intracellular Cl^- is extruded through the K^+-Cl^- cotransporter (KCC2; Rivera et al., 1999), the driving force for Cl^- ions is inverted, so that activation of GABA receptors generates an outward hyperpolarizing (i.e. inhibitory) current.
In the cerebellar interneuron network, inhibitory and excitatory GABA connections coexist also at late developmental stages (Chavas and Marty, 2003). The reversal potential of GABAergic currents measured in interneurons of juvenile (P12-14) and subadult (P20-25) rats is relatively depolarized and contrasts with the hyperpolarized value for Purkinje cells (-58 mV and -85 mV, respectively). This average value close to the resting membrane potential of interneurons implicates that GABAergic transmission may exert excitatory effects in some stellate cells and inhibitory effects in other stellate cells, depending on the actual intracellular concentration of Cl^-.

For the sake of simplicity we will refer to GABA transmission as inhibitory in the following discussion, also considering that our experimental conditions (low intracellular Cl^- and depolarized holding membrane potential, see Methods) allow us indeed to record hyperpolarizing GABAergic currents. Nevertheless, especially when discussing the physiological consequences of the presented effect, one has to consider that the equation GABAergic = inhibitory is not always true in the cerebellar interneuron network.

1.3 Aim of the project

The GABAergic interneurons in the molecular layer play a pivotal role in the cerebellar circuitry since they balance the excitation that Purkinje cells receive from parallel fibers and climbing fibers, thereby modulating the final output of the cerebellum.

Recent studies indicate that inputs from the somatosensory system induce in the cerebellum a form of enhanced release of glutamate, which results from high frequency firing of granule cells (Chadderton et al., 2004), and this can induce phenomena of long term plasticity at excitatory synapses onto stellate cells and basket cells (Smith and Otis, 2005; Soler-Llavina and Sabatini, 2006). Such modifications of the glutamatergic pathway affect the excitability of the interneurons, and modulate indirectly the action potential dependent release of GABA from these cells. In addition to this, other studies have attempted to find a direct effect of glutamate on the GABA release by raising the idea that glutamate receptors are also localized in the axon terminal of cerebellar interneurons (Bureau and Mulle, 1998; Glitsch and Marty, 1999) and can be activated by spillover of glutamate (Satake et al., 2000, 2004). However, a clear view about the physiological relevance of these effects is still lacking, since most of these studies were performed using instead of release of endogenous glutamate application of exogenous agonists, which does not reproduce in vivo conditions.

We investigated the effect of sustained glutamatergic activity at the level of single synaptic connections between GABAergic interneurons in acute cerebellar slices from mice.

We restricted our study to the stellate cell network where only two types of synaptic inputs are involved (glutamatergic input from granule cells and inhibitory input from stellate cells), which makes it a suitable system for studying effects of cross talk between excitatory and inhibitory synapses.

We established electrophysiological protocols ensuring stable recordings and attempting to reproduce physiological conditions. Electrical activity between synaptically connected interneurons was monitored by double patch-clamp recordings and release of endogenous

glutamate from granule cells was induced by train stimulation in the granule cell layer. The involvement of specific receptors in mediating the effects on synaptic transmission was tested with pharmacological tools.

2. METHODS

2.1 The patch-clamp technique

The electrical activity of individual neurons can be recorded with the patch-clamp technique developed by Neher and Sakmann (Neher and Sakmann, 1976; Hamill et al., 1981). The main principle is that a tight seal (giga-seal) is formed between a glass pipette and the membrane of a neuron. This configuration allows measuring of the small currents and voltages (in the range of picoampere and microvolt) that are involved in neuronal activity, with a low electrical background noise. Originally developed to measure the currents flowing through single ion channels (Neher and Sakmann, 1976; Brenner and Sakmann, 1978), the patch-clamp, especially in the whole-cell configuration, has been very useful to measure and control the electrical activity of individual neurons (Stuart and Sakmann, 1994; Markram et al., 1995; Schiller et al., 1995) and of synaptically coupled pairs of neurons (Markram et al., 1997) in acute brain slices.

2.1.1 Experimental patch-clamp setup

Electrical recordings from cerebellar stellate neurons were performed with the double patch-clamp amplifier EPC-10 (HEKA, Lambrecht, Germany) operated in voltage clamp mode.
Acute cerebellar slices from anesthetized mice were placed in a recording chamber constantly perfused with oxygenated artificial cerebrospinal fluid (ACSF) under an upright microscope stage (Axioskop 2, Zeiss, Jena, Germany) equipped with a 5x objective (Plan-Neofluar, Zeiss), a 40x objective (IR-Achroplan, Zeiss) combined with 1.6x magnification. Stellate cells were identified in the outer molecular layer of the cerebellum by infrared differential contrast optics using an infrared-sensitive video camera (C2400, Hamamatsu, Japan).
The preamplifier headstages holding the patch pipettes were mounted on three axis motorized micromanipulators (Luigs&Neumann, Ratingen, Germany) allowing precise control of the position of the pipette tip. Pressure or suction could be applied to the pipette by a manual seal sucker (Sigmann Elektronic, Hüffenhardt, Germany). A third micromanipulator was equipped with a pipette holder connected to a stimulation isolator (WPI, Saratosa, USA) for extracellular stimulation. The micromanipulators together with the slice recording chamber were mounted on a motorized xy-translation table. In this way, the sample together with the patch electrodes could be moved below the fixed optical axis of the microscope. The brain

slice in the recording chamber was fixed with a grid made of a platinum frame spanned with dental floss. The extracellular medium was grounded with a Ag/AgCl pellet via the reference input of the preamplifier headstage. The solution in the patch pipette was in electrical contact with the preamplifier via a chlorinated silver wire.
The complete setup was mounted on a vibration isolation table (Newport, Irvine, CA, USA) to minimize vibrations. In order to minimize electrical noise during the recording the electrical setup was surrounded by a Faraday cage and all setup components were carefully grounded.

2.1.2 Patching

The "blow and seal" technique was developed by Stuart and Sakmann to form a high resistance seal onto the soma of a neuron in a brain slice (Stuart et al., 1993). The individual steps of the patch-clamp technique are depicted in Fig. 2.1. Briefly, the patch-clamp amplifier is set to the voltage clamp mode and a command voltage pulse of –5 mV and 10 ms duration is continuously applied to the electrode. In the voltage clamp mode the amplifier keeps the voltage at the set value and measures the resulting current. Positive pressure is applied to the pipette to keep the tip clean from dirt, a prerequisite for successful formation of a giga-seal.
From the amplitude of the current response to the –5 mV voltage step the pipette tip resistance can be calculated applying Ohm's law. Pipette resistance was usually between 5-8 MΩ. When the pipette is lowered onto the top of the slice, the potential of the bath solution is set to 0 mV. The pipette tip is then targeted to the soma of a neuron selected under visual control. As soon as the pipette penetrates the brain slice, a wave of pressure can be seen in the slice clearing the surface of the targeted neuron. The pipette is slowly advanced to the soma until a dimple in the cell membrane becomes visible. Then the pressure is released and slight suction is applied. The membrane starts to seal onto the tip of the pipette. This process can be observed in the electrical current recording. The initial command voltage is set to –60 mV. The leak current from the tip of the pipette then decreases rapidly within a few seconds to a few pA. This corresponds to the formation of a high resistance seal (in the GΩ range) between the cell membrane and the pipette. Since the membrane acts as a capacitor, transient capacitive currents can be observed when the command voltage is stepped to –5 mV and back to ground potential. The amplifier is equipped with circuits that can compensate for the membrane capacitance and the pipette resistance.

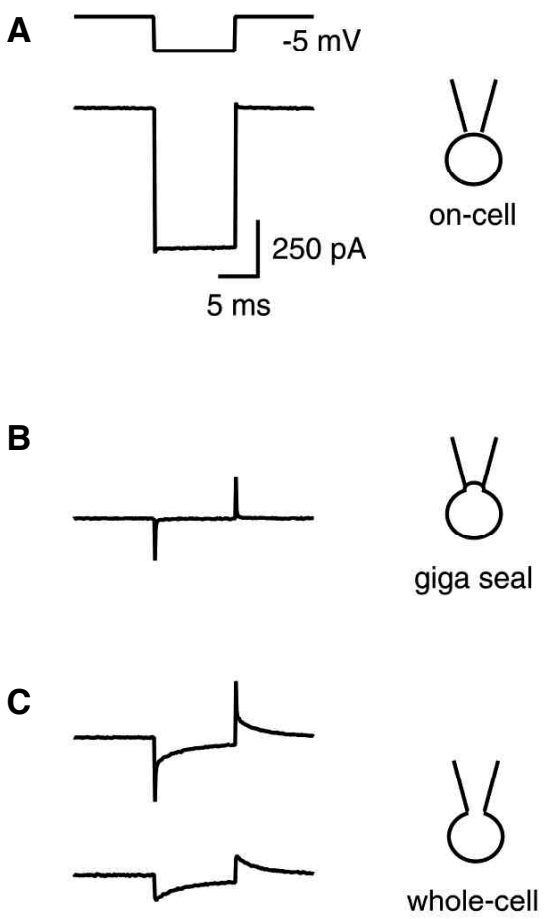

Figure 2.1 ***The patch-clamp technique***

Formation of a giga-seal and whole-cell configuration.
A The cell soma is approached by a patch pipette. The current through the pipette in response to a voltage step is recorded. Positive pressure applied to the pipette keeps the tip clean and causes a "dimple" in the plasma membrane.
B The pressure is released and slight suction results in the formation of a giga-seal. The resistance between the pipette and the bath solution is in the order of GΩ and no measurable current is flowing.
C The voltage command is set to –60 mV and brief suction is applied to disrupt the membrane patch below the pipette tip and to establish the final whole-cell configuration. The capacitative transients are compensated.

After the giga-seal is established, a transient suction pulse disrupts the membrane below the pipette without disrupting the tight seal. This whole-cell configuration now gives good electrical access to the cell. The pipette and the lumen of the neuron represent one electrical compartment, which can be modeled by an equivalent circuit (Sigworth et al., 1995) as shown in Fig. 2.2. Typical values for membrane capacitance, series resistance and membrane resistance for cerebellar stellate cells are $C_m \sim 5$ pF, $R_s \sim 15$ MΩ, $R_m \sim 1$ GΩ.

The amplifier was then routinely switched to the voltage-clamp mode. In voltage-clamp the membrane potential is kept constant and the current flowing through the membrane is measured. The command voltage was set at –60 mV, which is close to the resting membrane potential (i.e. without electrical activity) of cerebellar interneurons. Brief depolarizing voltage pulses can excite the cell and result in the firing of an action current.

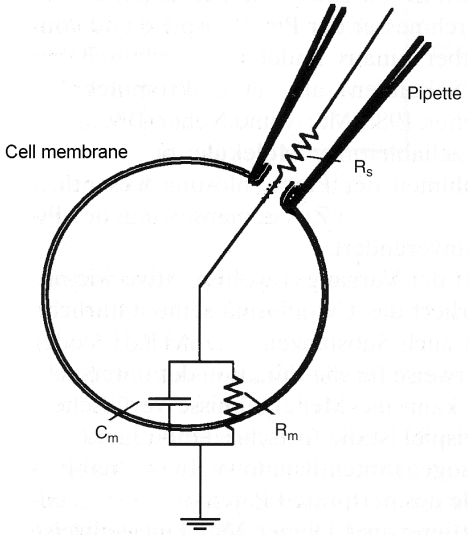

Figure 2.2 ***Equivalent circuits for whole-cell configuration***

In the whole-cell configuration, the passive electrical properties of the cell can be simply represented as a capacitor (C_m) in parallel to a resistor (R_m). A further series resistance (R_S) originates at the contact between the electrode and the cell cytoplasm. (Adapted from Numberger and Draguhn, 1996)

2.1.3 Slice preparation

Acute cerebellar slices (250 μM thick) in the sagittal plane were prepared from C57/BL6 mice. 13-15 day-old (P13-15) or 19-26 day-old (P19-26) mice were deeply anesthetized with halothane (Eurim-Pharm, Piding, Germany) or isofluran (Baxter, Germany). The cerebellum was removed and placed in ice cold ACSF, containing (in mM): 125 NaCl, 25 $NaHCO_3$, 2.5 KCl, 1.25 NaH_2PO_4, 1 $MgCl_2$, 25 Glucose, 2 $CaCl_2$ (Biometra, Göttingen, Germany), bubbled with 95% O_2 / 5% CO_2. The cerebellar vermis was separated from the hemispheres with a razor blade, glued with cyanoacrylate glue (UHU, Germany) with the cut surface facing down onto a metal plate, which was tightly fixed in a slicing chamber. 250 μm thick slices were prepared using a vibratome (Sigmann Elektronik, Hüffenhardt, Germany) with a razor blade at an angle of 12° to horizontal. The slicing chamber contained an oxigenated ice cold solution composed of (in mM): 140 K-Gluconate, 10 Hepes, 15 Na-Gluconate, 0.2 EGTA, 4 NaCl. The slices were transferred to a recovery chamber containing ACSF and allowed to recover for 30 min at 35° before recording. All experiments were performed up to 6 hours after slicing.

2.1.4 Pipettes

Patch and stimulation pipettes were pulled from borosilicate glass capillaries (Hilgenberg, Malsfeld, Germany) on a horizontal pipette puller (P97, Sutter Instruments, Novato, CA, USA).

2.1.5 Solutions

Synaptically connected stellate cells were patched with patch pipettes (5-8 MΩ) filled with an intracellular solution containing (in mM): 130 K-Gluconate, 10 Hepes, 10 Phosphocreatine, 10 Na-Gluconate, 4 MgATP, 0.3 GTP, 0.2 EGTA, 4 NaCl (pH corrected to 7.2 with KOH, 290-305 mOsm). For the postsynaptic cell QX-314 (2.5 mM) was added to the intracellular solution to block the voltage gated Na^+ channels. The stimulation pipette was filled with ACSF.

During the electrophysiological recordings the slices were constantly perfused with oxigenated ACSF (composition see above) at room temperature. In experiments with pharmacological tools the drugs were continuously present in the extracellular medium, with the exception of GYKI 53655 or SKF-89976A, that were added to ACSF and perfused by a peristaltic pump (IPC-8, Ismatec, Glattbrugg, Switzerland) after the extracellular stimulation in the granule cell layer was established. For minis recordings, the agonists were applied by superfusion with the peristaltic pump.

2.1.6 Data acquisition and Analysis

The current signals were filtered at 3 kHz and digitized at 10 kHz by the on-board AD-converter of the EPC-10 (ITC-16, Instrutech, Great Neck, NY, USA). The amplifier and the ITC-16 were both controlled by the program Patchmaster (version 1.12, Heka Elektronik, Lambrecht, Germany) on a Macintosh PowerPC G4 (Apple, Cupertino, CA, USA). Peak amplitudes of eIPSCs were analyzed off-line with the Patchmaster analysis macro. Calculation of average peak amplitude, failure rate and paired-pulse ratio were performed using Excel (Microsoft Corp., USA). Miniature events were detected and analyzed using a macro written for Igor (Wavemetrics Inc., USA). The detection threshold was set at 4-5 pA. All software-detected IPSCs were inspected by eye and peaks that did not resemble IPSCs were rejected.

Data are presented as mean ± SEM. Statistical significance was evaluated by paired Student's *t*-test and with ANOVA performed with GB-Stat 5.0.6 (Dynamic Microsystem Inc, Silver Spring, USA). Significance levels were set below p = 0.05 and indicated by asterisks (* = p < 0.05; ** = p < 0.01).

2.2 Double patch recordings

2.2.1 Stimulation protocol

Double patch recordings from synaptically connected stellate cells were performed using the following procedure:

1. A stellate cell was patched usually in the middle of the molecular layer and held at –35/–40 mV in voltage-clamp mode of the whole-cell configuration. Fig. 2.3 shows a representative recording of the spontaneous activity in a stellate cell. With low intracellular concentration of Chloride (6.5 mM) $GABA_A$ receptor mediated sIPSCs are recorded as outward currents, which can be univocally distinguished from the AMPA receptor mediated inward sEPSCs.

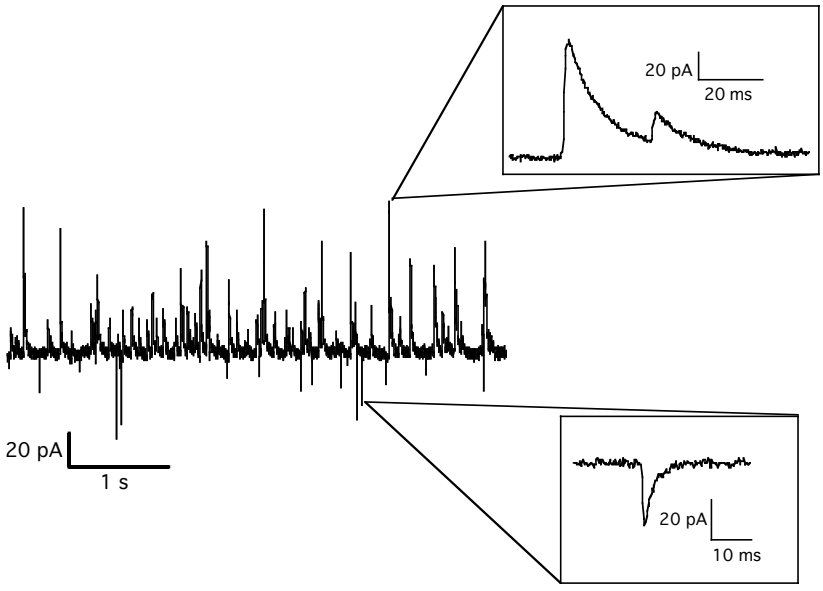

Figure 2.3 ***Recording of spontaneous activity***

Spontaneous activity recorded in a stellate cell that was voltage-clamped at -40 mV. $GABA_AR$ mediated sIPSCs appear as outward current (upper inset), whereas iGluR mediated events are inward (lower inset).

2. A putative presynaptic stellate cell was chosen in the surrounding layer up to 100 μm away from the already patched cell. A cell-attached patch was established, which allows recording of the spontaneous firing of the neuron. The two cells were synaptically connected if a correlation between the spiking of the putative presynaptic cell and IPSCs of the postsynaptic cell occurred, as depicted in Fig. 2.4.

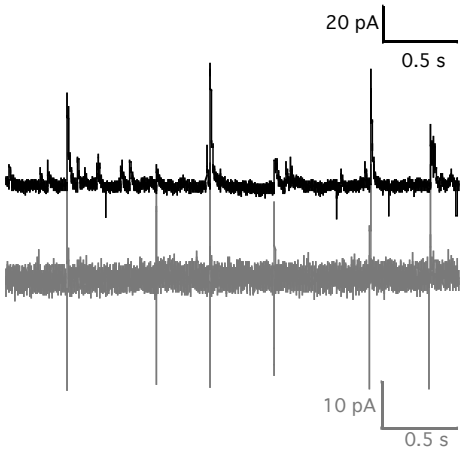

Figure 2.4 ***Recording of spontaneous activity in two stellate cells***

The postsyaptic cell is held in voltage-clamp mode at -40 mV (black trace), the putative presynaptic cell is clamped in the cell-attached mode (gray trace). Correlation of the presynaptic firing with the postsynaptic IPSCs reveals that the interneuron pair is synaptically connected.

3. The presynaptic cell was brought into whole-cell configuration and voltage-clamped at –60 mV.

$GABA_A$ receptor mediated IPSCs were evoked by stimulating the presynaptic cell with brief voltage steps (0.5-1 ms) from –60 mV to 0 mV. This produces unclamped spikes, corresponding to large depolarizing Na^+ currents (Fig. 2.5), that can be followed in some cases by small hyperpolarizing K^+ channel currents, depending on the pulse length (see for example Fig. 2.7). To test for short term plasticity, a paired-pulse paradigm with 20 ms interval was performed.

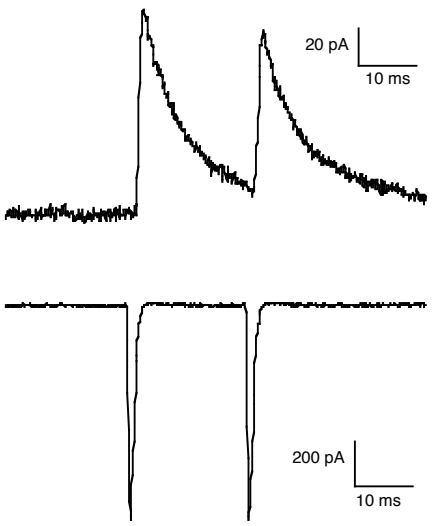

Figure 2.5 ***Stimulation protocol for eIPSCs***

Unclamped action currents (lower trace) were generated in the presynaptic cell by brief voltage steps (from –60 mV to 0 mV for 0.5-1 ms) in a 20 ms paired-pulse paradigm. The responses in the postsynaptic cell voltage-clamped at –35 mV appear as outward currents (upper trace).

A schematic drawing of the recording condition in cerebellar slices is depicted in Fig. 2.6. Glutamate was released by stimulating the granule cell layer with an extracellular pipette. The stimulation strength was adjusted to produce a large and reproducible response in the stellate cells upon a train of stimuli (see below).

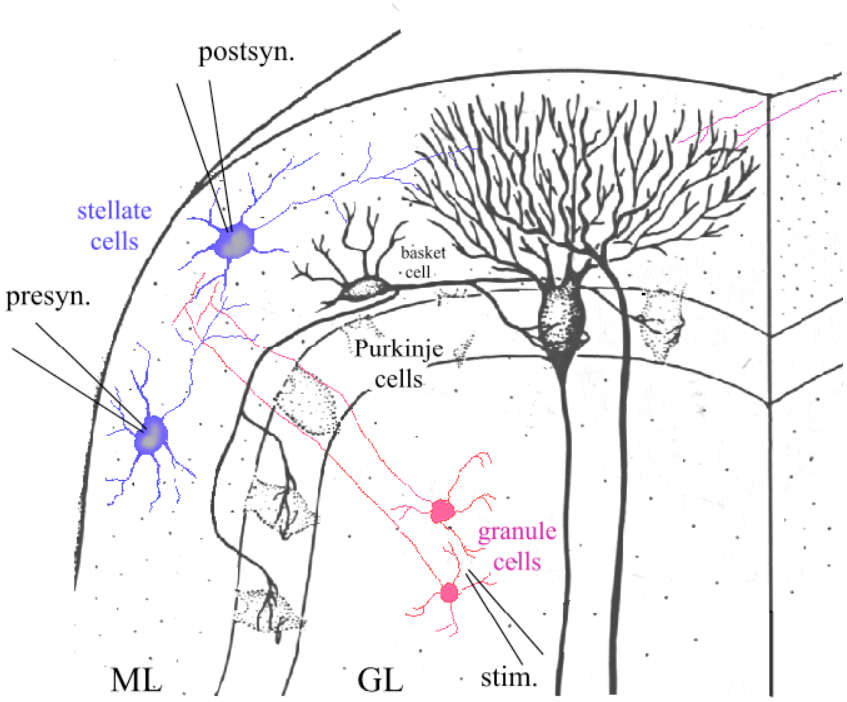

Figure 2.6 ***Double-patch recording from stellate cells and extracellular stimulation in granule cell layer***

Schematic drawing of a cerebellar slice in the sagittal plane. Two connected stellate cells in the molecular layer (ML) are patched, and granule cells are stimulated in the granular layer (GL) with an extracellular stimulation pipette.

The stimulation protocol consisted of three steps (Fig. 2.7):

A) test responses in a 20 ms paired-pulse paradigm were evoked in the stellate cells pair.

B) after 10 s a train of 30 stimuli at 50 Hz was generated in the granule cell layer.

C) 40 ms after the end of the train conditioned responses were evoked in the stellate cell pair.

This series was repeated every 20 s for at least 15 times.

Test responses and conditioned responses were averaged and compared.

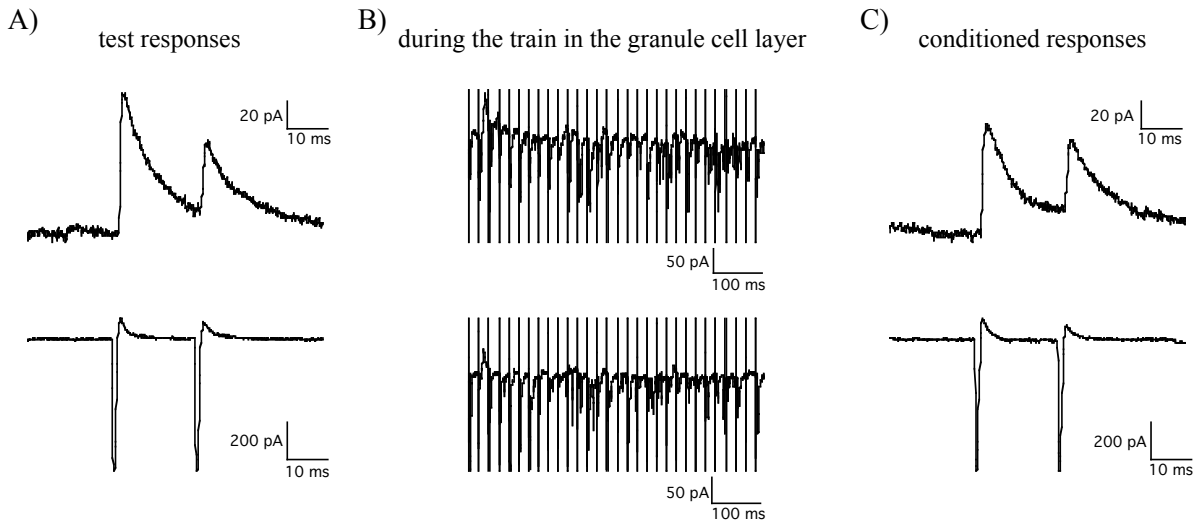

Figure 2.7 ***Stimulation protocol***

A) Test responses were generated in the postsynaptic cell (upper trace) by eliciting firing of the presynaptic cell (lower trace) in a 20 ms paired-pulse paradigm. Post- and presynaptic cell were voltage-clamped at –35 mV and –60 mV, respectively. B) After 10 seconds train stimulation (50 Hz frequency) was elicited in the granule cell layer. This generated eEPSCs and eIPSCs in the stellate cell pair. C) Conditioned responses were generated in the interneuron 40 ms after the end of the train. This series was repeated every 20 s for 15 times.

2.2.2 Synaptic Rundown

In double patch experiments the presynaptic cell was patched in the whole-cell configuration. This has been shown to lead to an irreversible decline of the synaptic strength occurring within 10-20 min of recording (Diana and Marty, 2003). This synaptic rundown originates from the fact that the dialysis of the intracellular compartments via the patch pipette causes the washout of substances involved in neurotransmitter storage and release.

Therefore, unlike usual protocols, in which first a series of test responses and then a series of conditioned responses are performed, test and conditioning were performed in each single stimulation series, so that they would be affected in parallel by the rundown.

Furthermore, the last series of the recorded responses were discarded from the analysis if the synapse was affected by a dramatic rundown (more than 50% reduction of the test responses).

2.3 Two-photon Microscopy

2.3.1 Principles of fluorescence excitation

Fluorescence imaging is a powerful tool in biology to enhance contrast, label individual proteins or structures and perform functional imaging of ionic concentrations or membrane potential. Fluorescence techniques are well matched to problems in neurobiology. Whenever possible, neurons need to be studied in their natural habitat, and intact brain tissue is an especially challenging place for light microscopy. In wide-field fluorescence microscopy, contrast and resolution are degraded by strong scattering (Denk and Svoboda, 1997). Confocal microscopy can overcome some of the effects of scattering, since the detector pinhole rejects fluorescence from off-focus locations (Conchello and Lichtman, 2005; Denk and Svoboda, 1997). However, scanning a single section excites, and thereby damages, the entire specimen. Furthermore, the pinhole also rejects signal photons emanating from the focus that are scattered on their way out of the tissue. Deep in tissue, confocal microscopy becomes unacceptably wasteful in terms of signal photons (Centonze and White, 1998; Conchello and Lichtman, 2005). Compensating for signal-loss with increased fluorescence excitation leads to phototoxicity and photobleaching. Wide-field and confocal microscopy are thus techniques that are best applied to thin specimens, such as cultured preparations or the most superficial cell layer in a tissue (< 20 μm) (Lichtman et al., 1987). Experiments deeper in tissue benefit from two-photon excitation (2PE; also referred to as two-photon, or multiphoton) microscopy, which allows high-resolution and high-contrast fluorescence microscopy deep in the brain (for review see Svoboda and Yasuda, 2006). Two-photon excitation was first described theoretically by Göppert-Mayer in 1931 (Göppert-Mayer, 1931). Because the probability for two-photon excitation is very small, the experimental observation was first possible with the introduction of short-pulse lasers, a source of high intensity photon fluxes (Spence et al., 1991). In 1990 Denk et al. described two-photon excitation fluorescence microscopy for imaging biological specimens (Denk et al., 1990).

2.3.2 Principles of Two-photon Excitation Microscopy

Fluorescence is generated when a molecule is electronically excited from its ground state to an excited state by absorption of a photon of the corresponding energy and then relaxes rapidly (t ~ 1 ns) by emission of a red-shifted photon again to its ground state. In 2PE of

fluorescence, two low-energy photons cooperate to cause a higher-energy electronic transition in a fluorescent molecule (Fig. 2.8A). 2PE is a nonlinear process in that the absorption rate depends on the second power of the light intensity. In a focused laser, the intensity is highest in the vicinity of the focus and drops off quadratically with distance above and below. As a result, fluorophores are excited almost exclusively in a tiny diffraction-limited focal volume (Fig. 2.8B). If the beam is focused by a high numerical aperture (NA) objective, the vast majority of fluorescence excitation occurs in a focal volume that can be as small as 0.1 μm^3 (Zipfel et al., 2003).

The key consequence of localization of excitation is three-dimensional contrast and resolution (comparable to confocal microscopy) without the necessity for spatial filters in the detection path (e.g., the detector pinhole in the confocal microscope) (Wilson and Sheppard, 1984; Denk et al., 1990). To generate an image, the laser is scanned over the specimen. Since the excitation occurs only in the focal volume, all fluorescence photons captured by the microscope objective constitute useful signals. When imaging in thick specimens, the signal yield per excitation event is enhanced (Fig. 2.8B).

The properties of 2PE discussed so far are independent of scattering (Denk et al., 1990). When excitation photons enter tissue, their paths are altered by inhomogeneities in the index of refraction (Denk et al., 1994; Denk and Svoboda, 1997; Helmchen and Denk, 2005). Depending on the type and age of the tissue and the wavelength of the light, about half of the incident photons are scattered every 50–200 μm (Oheim et al., 2001; Yaroslavsky et al., 2002; Kleinfeld et al., 1998). The scattering of excitation light effectively reduces the light delivered to form the diffraction-limited focus (Fig. 2.8B). Scattering also perturbs the trajectories of fluorescence photons on their way out of the tissue (Fig. 2.8C).

Compared to one-photon techniques, 2PE provides three key advantages for microscopy in scattering specimens (Denk et al., 1994). First, the excitation wavelengths used in 2PE microscopy, deep red and near IR, penetrate tissue better than the visible wavelengths used in one-photon microscopy. This improved penetration (up to 1 mm) is due to reduced scattering and reduced absorption by endogenous chromophores (Oheim et al., 2001; Svoboda and Block, 1994; Yaroslavsky et al., 2002). Second, because of the nature of nonlinear excitation, scattered excitation photons are too dilute to cause appreciable fluorescence (Fig. 2.8B). Even deep in tissue, under conditions where most of the incidence photons are scattered, excitation is therefore still mostly limited to a small focal volume. Third, because of localization of excitation, all fluorescence photons, ballistic and scattered, constitute useful signal if they are detected (Fig. 2.8B). In contrast, in wide-field and confocal microscopy, scattered

fluorescence photons are either lost or may contribute to background (Centonze and White, 1998). Since in typical experiments in tissue the majority of fluorescence photons are scattered, this advantage of two-photon microscopy can be huge.

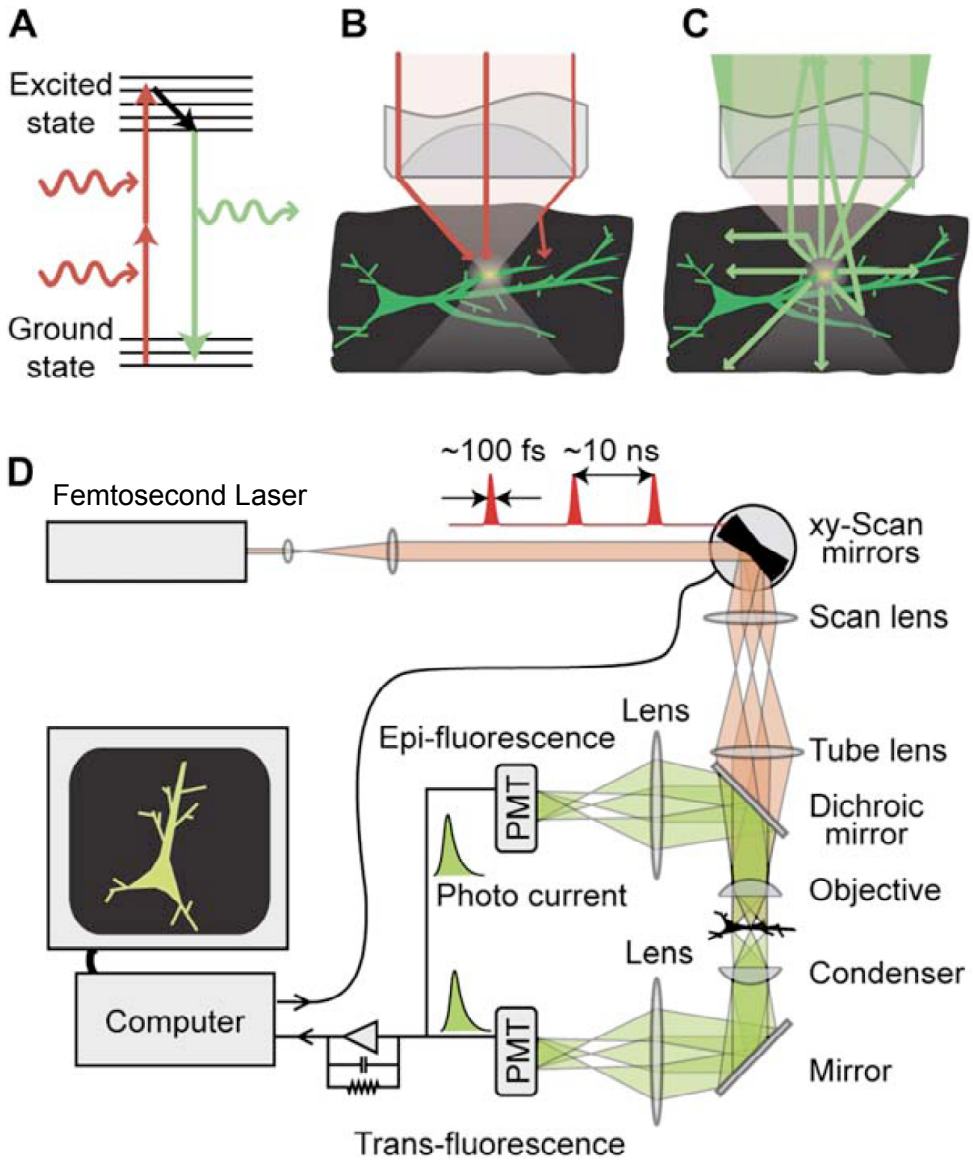

Figure 2.8 ***Principles and setup for 2PE (from Svoboda and Yasuda, 2006)***
A) Simplified Jablonski diagram of the 2PE process.
B) Localization of excitation in a scattering medium (black). The excitation beam (red) is focused to a diffraction-limited spot by an objective where it excites green fluorescence in a dendritic branch, but not in a nearby branch. The paths of two ballistic photons and one scattered photon are shown (red lines). Scattered photons are too dilute to cause off-focus excitation. The intensity of the beam decreases with depth as an increasing number of excitation photons are scattered.
C) Fluorescence collection in a scattering medium. Fluorescence photons are emitted isotropically from the excitation volume (green lines). Even scattered fluorescence photons contribute to the signal if they are collected by the objective. Since the field of view for detection is larger than for excitation, the fluorescence light exiting the objective back-aperture will diverge substantially. D) Schematic of a 2PE microscope with epifluorescence and transfluorescence detection.

2.3.3 Ca^{2+} imaging in axons of stellate cells

Ca^{2+} is an important second messenger to trigger many signaling cascades in neurons. In the axon terminal, the depolarization induced by an action potential leads to influx of Ca^{2+} through voltage gated Ca^{2+} channels, which triggers neurotransmitter release. Hence Ca^{2+} imaging in the axon of stellate cells provides a tool for estimating the amount of GABA released during evoked activity.

Functional imaging of Ca^{2+} influx is possible with a large number of Ca^{2+} ion sensitive indicator dyes. In order to do any Ca^{2+} measurement, neurons have to be loaded with a fluorescent Ca^{2+} indicator, which changes its properties upon binding Ca^{2+}. The indicator is in competition with endogenous Ca^{2+} binding proteins and it alters the decay time dynamics of the Ca^{2+} transients.

For Ca^{2+} imaging experiments, 2 mM CaCl were added to the extracellular ACSF to amplify the Ca^{2+} signals, and stellate cells were held in whole-cell mode using the intracellular solution described above supplemented with 100 μM of the K^+ salt of the Ca^{2+} sensitive dye Oregon Green 488 BAPTA-1 (Molecular Probes). A good labeling of the axon was reached after allowing the dye to diffuse into the cell for at least 30 min. The axon was distinguished from the dendrites by morphology (long and thin main branch running in the sagittal plane up to 200 μm with secondary branches extending in the perpendicular direction) and by functional criteria (presence of “hot spots”, i.e. local maxima in the Ca^{2+} responses, as described in Forti et al., 2000). Granule cell axons were labeled by electroporation of the cells with 500 μM Alexa Fluor 594 (Molecular Probes) contained in the stimulation pipette. Parallel fiber trunks were traceable after 3-5 repetitions of train stimulation. An example of a stellate cell filled with Oregon Green and granule cells axons loaded with Alexa is represented in Fig. 2.9.

Two-photon excitation was performed with a mode-locked 170 fs pulse Ti-Sapphire laser (Chameleon XR; Coherent, CA, USA) set at an excitation wavelength of 840 nm. The system used an upright Zeiss microscope equipped with a 63x water immersion objective (numerical aperture 1). Fluorescence signals were acquired with the LSM 510 software (Zeiss, Germany). Frame scan acquisition (150 frames) was performed from regions of interest (ROIs) set on the stellate cell axons in correspondence to hot spots of Ca^{2+} signals. ROIs had a size of 30 x 20 pixels (pixel size 40 nm x 40 nm) and were scanned with a rate of 30.27 ms (pixel dwell time = 1.28 μs) resulting in a time resolution of 33 ms. For background signal, a similar frame was

scanned in parallel in a nearby region not containing the axon. 4-9 ROIs were recorded per cell.

The stimulation protocol for Ca^{2+} imaging was based on the protocol for double patch recordings. Test Ca^{2+} transients were acquired upon firing of the cell elicited with paired-pulse voltage steps (from –60 to 0 mV, 0.5-1 ms, 20 ms interval) after a 500 ms baseline. For conditioned Ca^{2+} transients, train stimulation (30 stimuli, 50 Hz) was performed in the granule cell layer after 500 ms baseline and was followed by paired-pulse firing of the cell. Test responses and conditioned responses were alternatively acquired and averaged (two or three traces for each ROI). ROIs that showed rundown in the test responses, likely induced by photobleaching and/or photodamaging, were not considered.

Offline analysis of the fluorescence signals was performed using a macro written for Igor (Wavemetrics Inc., USA). Values are expressed as the percentage change in fluorescence with respect to baseline:

$$\frac{\Delta F}{F_0} = 100 \cdot \frac{F - F_0}{F_0 - B}$$

where F is the measured fluorescence signal at any given time, F_0 is the average from the prestimulus signal, and B is the value, at each time point, of the background fluorescence.

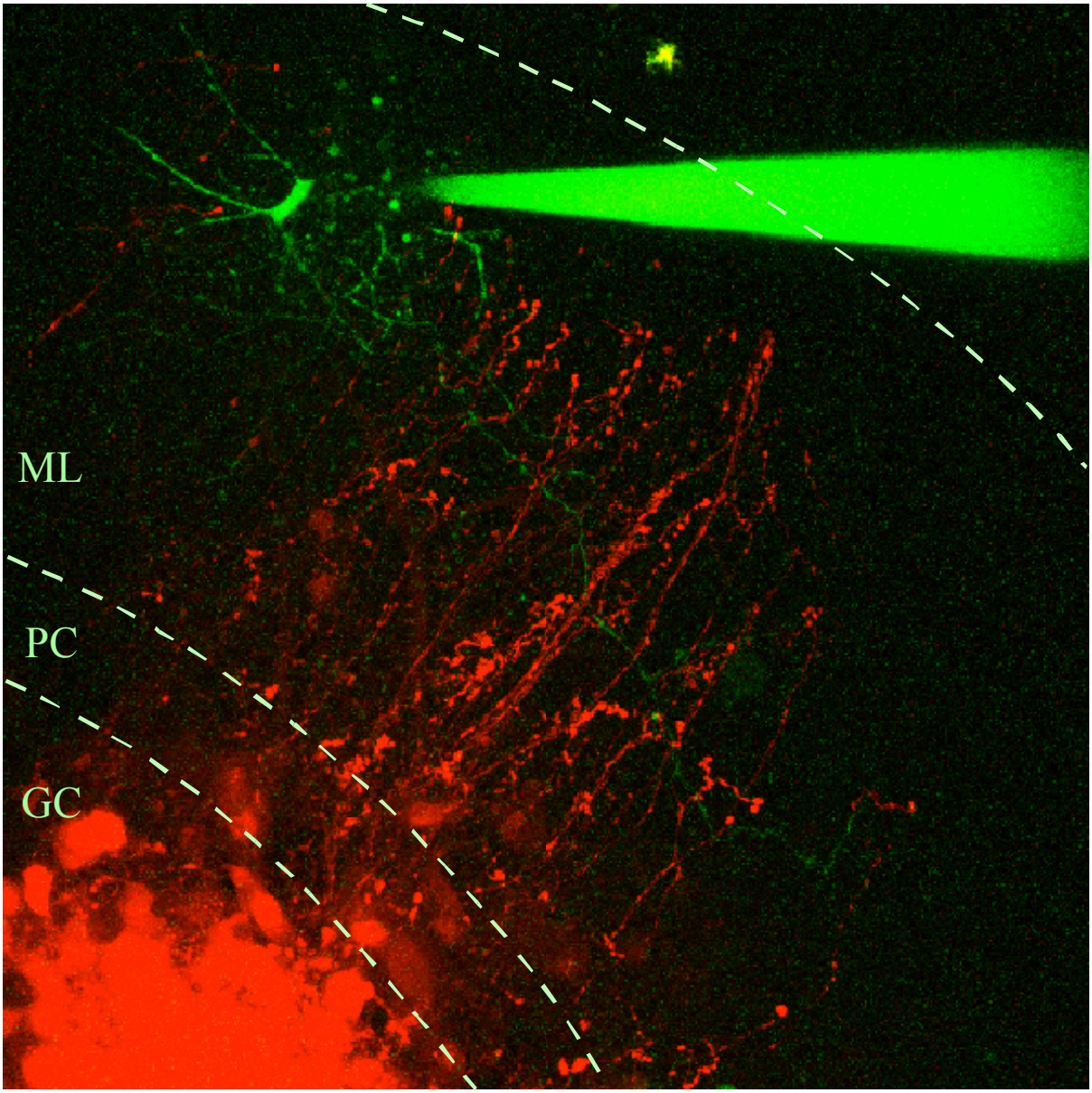

Figure 2.9 ***Loading of stellate cells and granule cells for Ca^{2+} imaging***

A stellate cell (in green) was loaded with 100 µM Oregon Green 488 BAPTA-1 contained in the patch pipette. The axon extends out of the dendritic region in a direction parallel to the Purkinje cell layer (PC). Granule cells (in red) were filled by electroporation achieved with repetitive stimulation (at least 5 x 30 stimuli at 50 Hz) in the granule cell layer (GC) with an extracellular pipette containing 500 µM Alexa Fluor 594. The axons run radially through the molecular layer (ML) before dividing into parallel fibers.
This picture is a z-projection elaborated by collecting the maximum intensity from 28 images taken in different focal planes with 1 µm intervals. Image size: 206.8 µm x 206.8 µm.

3. RESULTS

3.1 Paired recordings from cerebellar stellate cells

Double patch recordings were performed from synaptically connected cerebellar stellate cells in acute slices from P13-15 C57/BL6 mice. Stellate cells were visually identified in the molecular layer, and synaptic connections were found as described in Methods. GABAergic postsynaptic currents were evoked by applying short voltage pulses to the presynaptic neuron in the voltage-clamp mode (from –60 mV to 0 mV for 0.5-1 ms) in a 20 ms paired-pulse paradigm. The postsynaptic cell was voltage-clamped at –35/–40 mV and patched with a pipette containing a low concentration of Chloride (6.5 mM). This allows recording of large outwards GABAergic currents (eIPSCs = evoked Inhibitory PostSynaptic Currents), as shown in Fig. 3.1.

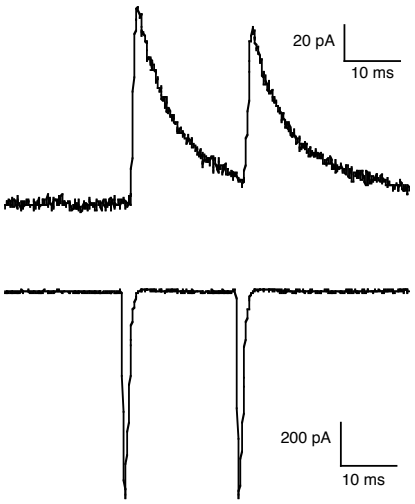

Figure 3.1 ***Double patch recording***

Activation of the presynaptic cell (bottom trace) with short voltage pulses (from –60 mV to 0 mV from 0.5 ms) in a 20 ms paired-pulse paradigm leads to release of GABA, which generates outward eIPSCs recorded at –40 mV in the postsynaptic cell (upper trace).

Stellate-to-stellate connections show a high variability in the synaptic responses (Kondo and Marty, 1998), reflecting the presence of single or multiple release sites. Average peak amplitudes of eIPSCs in different interneuron pairs ranged between 20-200 pA. For a single connection the paired-pulse ratio was estimated after averaging over many responses (>15). About 64% of the recorded synapses (n = 110) showed paired-pulse depression.

3.2 Glutamate mediated disinhibition at stellate-to-stellate synapses

We studied how the inhibitory GABAergic synapse between cerebellar stellate cells can be modulated by excitatory glutamatergic inputs provided by granule cells. For this aim, paired recordings from connected interneurons were established and test responses were compared with responses conditioned by the presence of glutamate released from the granule cells. The stimulation protocol was constructed in order to ensure stable recording conditions by minimizing the problem of synaptic rundown (§ 2.2.1 in Methods).

In P13-15 mice, glutamate released with a train of 30 stimuli at 50 Hz in the granule cell layer led to a reduction of the peak amplitude of the eIPSCs in stellate cell synapses. Fig. 3.2 shows a representative recording from one interneuron pair, whereas averaged normalized data from 8 different experiments are depicted in Fig. 3.3. The consequence of this effect is a reduction in the inhibitory input to stellate cells, which can be defined as *disinhibition*.

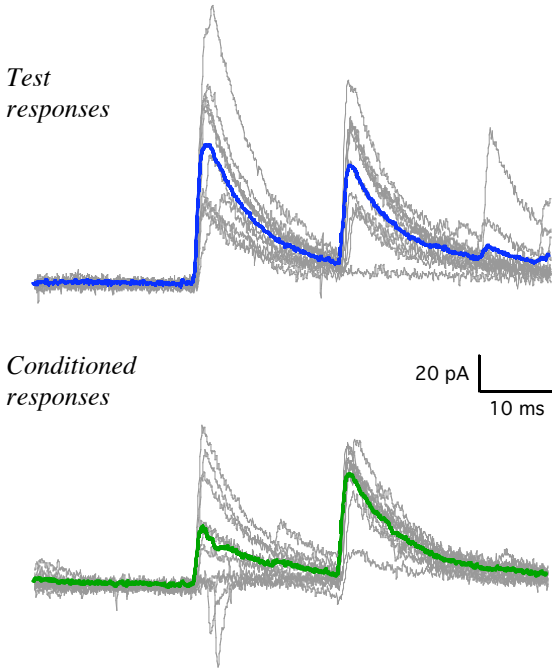

Figure 3.2 ***Disinhibition at a unitary connection***

Test responses and conditioned responses recorded from a single synaptic connection. The average of ten traces (in blue for test and in green for conditioned responses) shows the decrease in the amplitude of eIPSCs and the shift in the paired-pulse ratio towards facilitation. The increase in the failure rate in the conditioned responses is also noticeable.

In the paired-pulse paradigm the amplitudes of the first and second peak were significantly reduced by 28.0 ± 4.7 % ($p < 0.01$) and 19.5 ± 4.5 % ($p < 0.05$), respectively. Concomitantly, the failure rate was significantly increased in the conditioned responses (18.5 ± 5.7 % for the first peak and 18.0 ± 3.5 % for the second peak, compared to 6.3 ± 2.9 % and 8.0 ± 4.2 % in test responses, $p < 0.05$) and the paired-pulse ratio shifted towards facilitation (from 0.94 ± 0.05 to 1.08 ± 0.11).

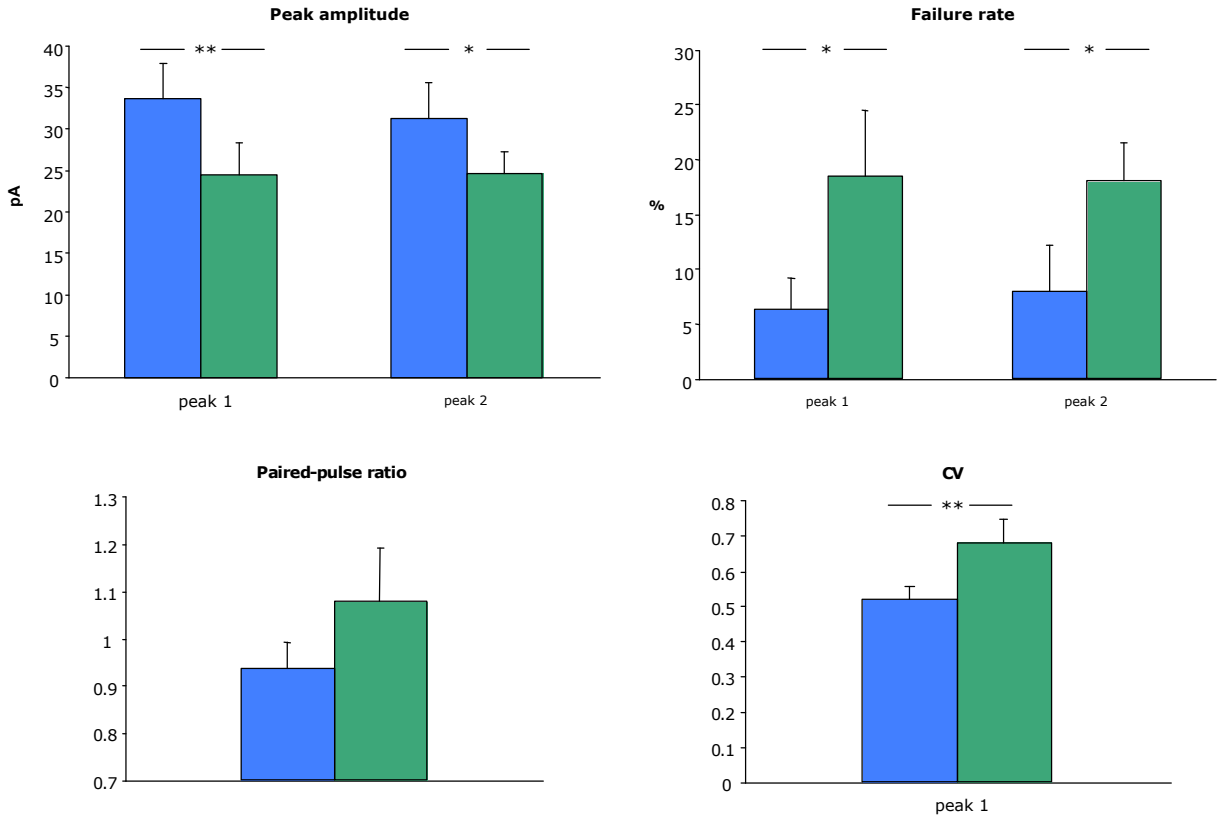

Figure 3.3 ***Disinhibition by change in release probability***

Effect of a train of 30 stimuli in the granule cell layer on average normalized peak amplitude, failure rate, paired-pulse ratio and coefficient of variation of eIPSCs evoked in 8 pairs of stellate cells. Blue and green bars indicate test responses and conditioned responses, respectively.

Changes in failure rate and paired-pulse ratio are commonly considered as an indication for presynaptic modification in transmitter release. This possibility was supported by the analysis of the coefficient of variation (CV), defined as standard deviation divided by mean amplitude of the eIPSCs. Assuming a simple binomial model to describe the transmitter release (Castillo and Katz 1954; Bekkers 1994), $CV = ((1-p)/np)^{-2}$ is a function of only presynaptic parameters, namely the number n of release sites and the release probability p of a single site and it is independent of the postsynaptic response q (Faber and Korn, 1991). The CV of the eIPSCs increased significantly from 0.52 ± 0.04 in test responses to 0.68 ± 0.07 in conditioned responses ($p < 0.01$).

3.2.1 Temporal characterization of the modulating effect

To study the temporal course of the glutamate driven effect on eIPSCs, a series of experiments was performed in which the conditioned responses followed the train stimulation in the granule cell layer with different time delays. In the standard protocol described above the first voltage pulse activating the firing of the presynaptic cell in the conditioned responses was generated 40 ms after the end of the train. In this new experimental series, a further delay of 50 ms, 500 ms, or 1 s was added after the train (Fig. 3.4). Using a 50 ms or 500 ms delay, a significant effect on the first peak of the eIPSCs was still present, but reduced in comparison to the standard protocol: 22.3 ± 5.4 % for 50 ms (n = 6) and 13.6 ± 4.5 % for 500 ms (n = 7), instead of 28.0 ± 4.7 % with no additional delay. Only a slight but still significant effect remained with 1 s delay (6.7 ± 1.8 %, n = 6). The reduction of the second peak of the paired-pulse was similarly affected, although the statistical significance was lost already with the 50 ms delay protocol. The values for the second peak were 17.0 ± 9.5 % for 50 ms, 10.6 ± 8.2 % for 500 ms, and 3.2 ± 2.2 % for 1 s delay.

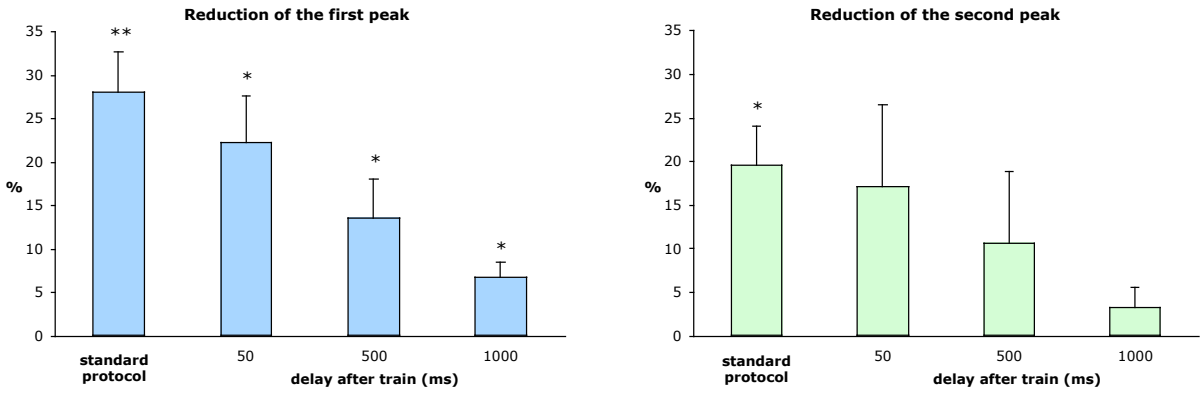

Figure 3.4 ***Temporal characterization of the disinhibitory effect***

Reduction of the first (left) and second (right) peak of paired-pulse eIPSCs using standard protocol and protocols in which a delay of 50 ms, 500 ms or 1000 ms was added after the train stimulation. The disinhibitory effect on eIPSCs declined with increasing time delay.

3.2.2 Pharmacological experiments

Glutamate released by a train of stimuli in the granule cell layer reduced the amplitude of eIPSCs in stellate cells by decreasing the release probability for GABA. In order to find out which receptors are involved in mediating this effect, we performed experiments with pharmacological tools and compared the reduction of the first peak of the paired-pulse to the value of the control experiment in absence of drugs using ANOVA statistics (Fig. 3.5).

The first step was to consider ionotropic receptors that are directly activated by glutamate, namely AMPARs and NMDARs.

When the specific AMPAR antagonist GYKI 53655 (50 μM) was added to the extracellular ACSF, the effect on eIPSCs was almost suppressed (5.1 ± 3.5 % reduction of the first peak, n = 8).

The involvement of NMDARs was ruled out by using the specific blocker APV (50 μM), which had no effect on the modulation of GABA release (24.9 ± 4.9 % reduction of the first peak, n = 7). This was confirmed by an opposite approach in which the activation of NMDARs was favored by lowering the extracellular Magnesium concentration (0.1 mM instead of 1 mM), which resulted in a reduction of 26.4 ± 4.9 % (n = 8).

We then tested whether the disinhibition could be explained by the involvement of endocannabinoids, which have been shown to play an important role in modulating synaptic transmission in the cerebellar interneuron network (Diana and Bregestovski, 2005). In our protocol they could be liberated from the surrounding Purkinje cells in response to the depolarization provided by the large amount of glutamate released during the train (Egertova et al., 1998; Tsou et al., 1998). However the CB1 receptor antagonist AM251 (2 μM) had no effect on the glutamate induced disinhibition (36.7 ± 4.5 % reduction of the first peak, n = 6).

The involvement of pre- and/or postsynaptic $GABA_B$ receptors (Mann-Metzer and Yarom, 2005) was tested by using the selective antagonist CGP-55845A (500 nM). In these experiments the peak amplitudes of eIPSCs were reduced by only 10.5 ± 4.6 % (n = 8), which was significantly different from the control experiment.

To test whether other metabotropic receptors are involved, we used a cocktail of blockers of metabotropic glutamate receptors (mGluRs) containing 300 μM AIDA, 500 μM (S)-MCPG and 500 μM CPPG, which antagonize unselectively group I, group I-II and group II-III of mGluRs, respectively. The reduction of eIPSCs was in this case 26.4 ± 3.8 % (n = 11), ruling out a contribution of mGluRs.

The analysis of paired-pulse ratio and coefficient of variation revealed the concomitance of the dishibinitory effect with a presynaptic modification in GABA release (Fig. 3.5). Although the statistical significance was not provided, a clear trend shows that the extent of the effect on peak amplitude of eIPSCs correlates with the change in paired-pulse ratio. In addition to this, the change in CV was significantly different from the control series in the experiments with AMPAR and $GABA_BR$ blockers, where also the disinhibitory effect was reduced.

To ensure stable recordings we mainly chose synaptic connections that gave rise to large eIPSCs. In these cases the occurrence of failures was rare in both control and conditioned responses, and the failure analysis was not performed.

Figure 3.5 (next page) ***Experiments with pharmacological tools***

Effects of the conditioning train on eIPSCs regarding peak amplitude of the first peak, paired-pulse ratio and CV calculated for the first peak, in different experimental conditions: control (no drug added to the extracellular medium), AMPAR blocker (50 µM GYKI 53655), NMDAR blocker (50 µM APV), 0.1 mM extracellular Mg^{2+}, cannabinoid receptor blocker (2 µM AM251), $GABA_B$ receptor blocker (500 nM CGP-55845A) and cocktail to block mGluRs (300 µM AIDA, 500 µM (S)-MCPG, 500 µM CPPG). Changes in paired-pulse ratio and CV were calculated as difference between the values for the conditioned responses and the values for test responses. Statistical significance compared to control experiment was tested using ANOVA with Fisher's LSD post hoc test (= $p < 0.05$; ** = $p < 0.01$).*

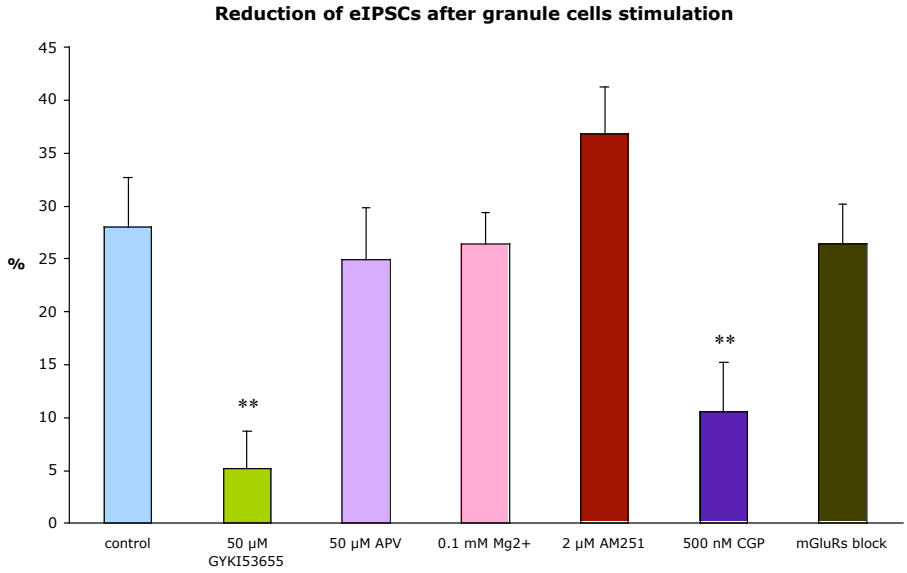
Reduction of eIPSCs after granule cells stimulation
%
45
40
35
30
25
20
15
10
5
0
**
**
control
50 µM GYKI53655
50 µM APV
0.1 mM Mg2+
2 µM AM251
500 nM CGP
mGluRs block

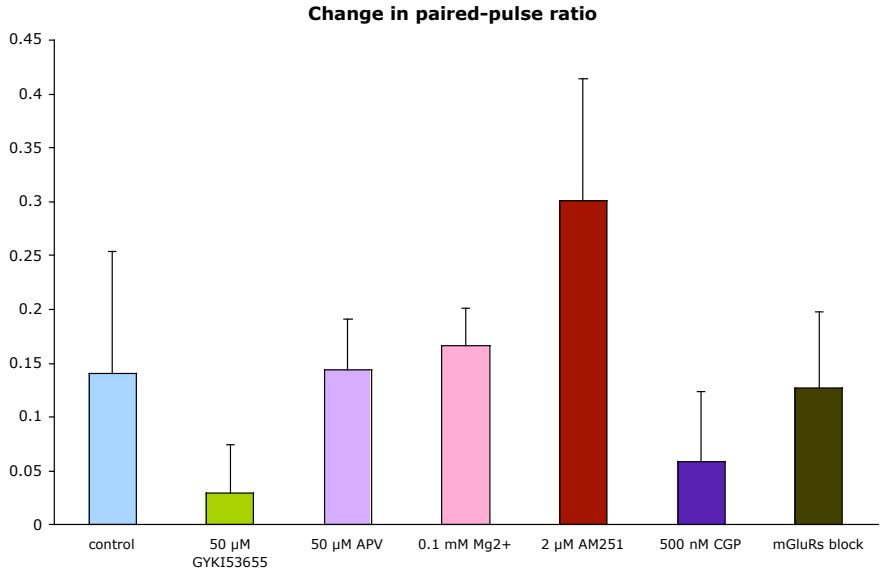
Change in paired-pulse ratio
0.45
0.4
0.35
0.3
0.25
0.2
0.15
0.1
0.05
0
control
50 µM GYKI53655
50 µM APV
0.1 mM Mg2+
2 µM AM251
500 nM CGP
mGluRs block

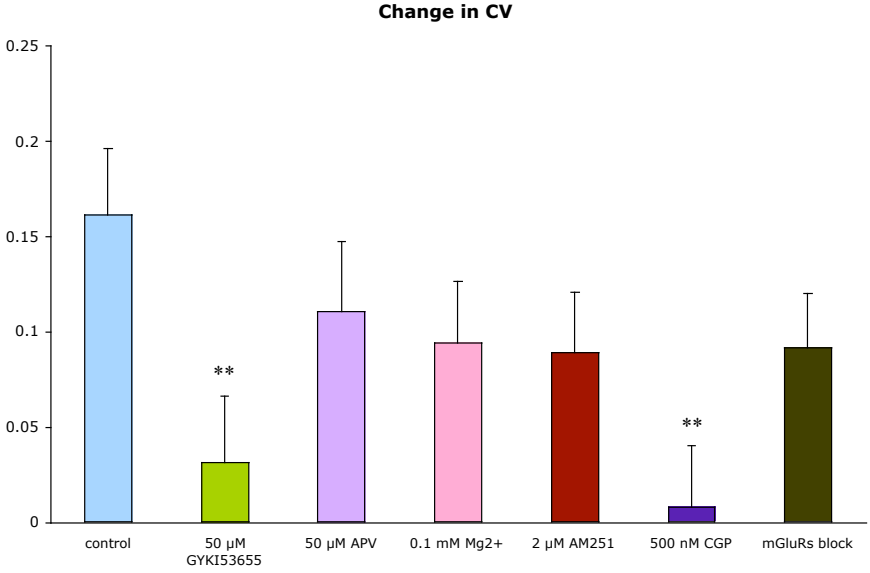
Change in CV
0.25
0.2
0.15
0.1
0.05
0
**
**
control
50 µM GYKI53655
50 µM APV
0.1 mM Mg2+
2 µM AM251
500 nM CGP
mGluRs block

3.2.3 Effects of AMPAR desensitization

The effect on evoked GABA release was maximal within a 50 ms temporal window after the conditioning train in the granule cell layer, suggesting that the disinhibition is directly controlled by the presence of neurotransmitter in the molecular layer. We therefore tested the consequences of boosting glutamate release by prolonged train stimulation.

Surprisingly, a train of 60 instead of 30 stimuli at 50 Hz in the granule cell layer resulted in a smaller effect on the eIPSCs (Fig. 3.6). The first peak of the paired-pulse was still significantly reduced by 17.6 ± 4.7 % (n = 10) and the effect was still sensitive to 50 µM GYKI 53655 (5.8 ± 4.4 % reduction, n = 12), confirming the involvement of AMPARs. To check the possibility that the larger amount of glutamate released by the longer train of stimuli induced desensitization of AMPARs, we repeated the 60 stimuli protocol in the presence of Cyclothiazide (CTZ, 25 µM), which inhibits AMPAR desensitization. The maximal effect was fully restored (35 ± 4 % reduction, n = 8).

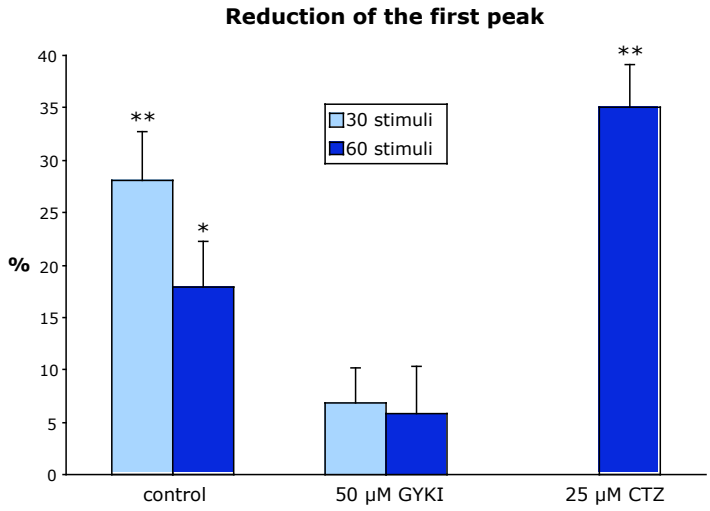

Figure 3.6 ***Effect of AMPAR desensitization***

A train of 60 stimuli (dark bars) instead of 30 (light bars) resulted in a smaller effect on eIPSCS, which could be restored by inhibiting the AMPAR desensitization with Cyclothiazide (25 µM).

3.2.4 Developmental regulation

The experiments described so far were performed in C57/BL6 mice of 13-15 days of age. To check whether the glutamate mediated disinhibitory effect undergoes changes during development, we examined 18-22 day-old animals. The 30 stimuli protocol resulted in a no longer statistically significant reduction of eIPSCs of 10.7 ± 4.7 % (n = 7), whereas with the 60 stimuli protocol the disinhibition was totally suppressed (0.3 ± 3.7 % reduction, n = 15), as shown in Fig. 3.7. Since the experiments characterizing the temporal course of the effect provided evidence that the temporal profile of the glutamatergic input plays a striking role in mediating the conditioning effect, the question arose, whether the actual presence of glutamate in three week-old mice could be modified by an improved transmitter uptake system (Grosche et al., 2002). This hypothesis was excluded by the fact that inhibiting the glutamate uptake system in three week-old mice with 50 µM TBOA did not result in a significant reduction of eIPSCs (5.8 ± 7.1 %, n = 6). The latter experiment was performed using the 30 stimuli protocol in the presence of 50 µM APV to avoid activation of extrasynaptic NMDARs.

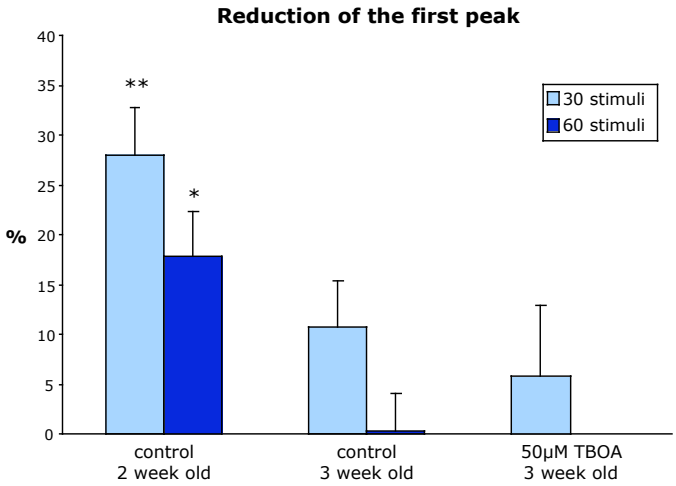

Figure 3.7 ***Developmental change***

The conditioning protocols with 30 stimuli (light bars) and 60 stimuli (dark bars) were performed in 2 week-old and 3 week-old mice. In a further experiment, the effect of the glutamate uptake inhibitor TBOA (50 µM, in addition to 50 µM APV) was tested in 3 week-old mice using the 30 stimuli protocol.

3.3 Activation of presynaptic receptors by transmitter spillover

The disinhibition at the synapses between stellate cells triggered by glutamatergic inputs from granule cells results from a modification occurring at a presynaptic level, namely a reduction in the GABA release, as indicated by the increase in failure rate, paired-pulse ratio and coefficient of variation. The application of pharmacological tools provided the evidence that at least two types of receptors are directly involved: AMPARs, because the effect was suppressed by the specific AMPAR antagonist GYKI 53655, and $GABA_B$ receptors, since the selective blocker CGP-55845A reduced the disinhibition by almost 50%. It has to be considered that a repetitive stimulation of granule cells liberates a large amount of glutamate, inducing spillover of the neurotransmitter in the surrounding molecular layer (Fig. 3.8A). Furthermore, other presynaptic stellate cells can be activated during the train stimulation, as indicated by eIPSCs generated in the postsynaptic cell during the train (Fig. 3.8B). Thus spillover of GABA can also be initiated, which may account for the involvement of $GABA_B$ receptors.

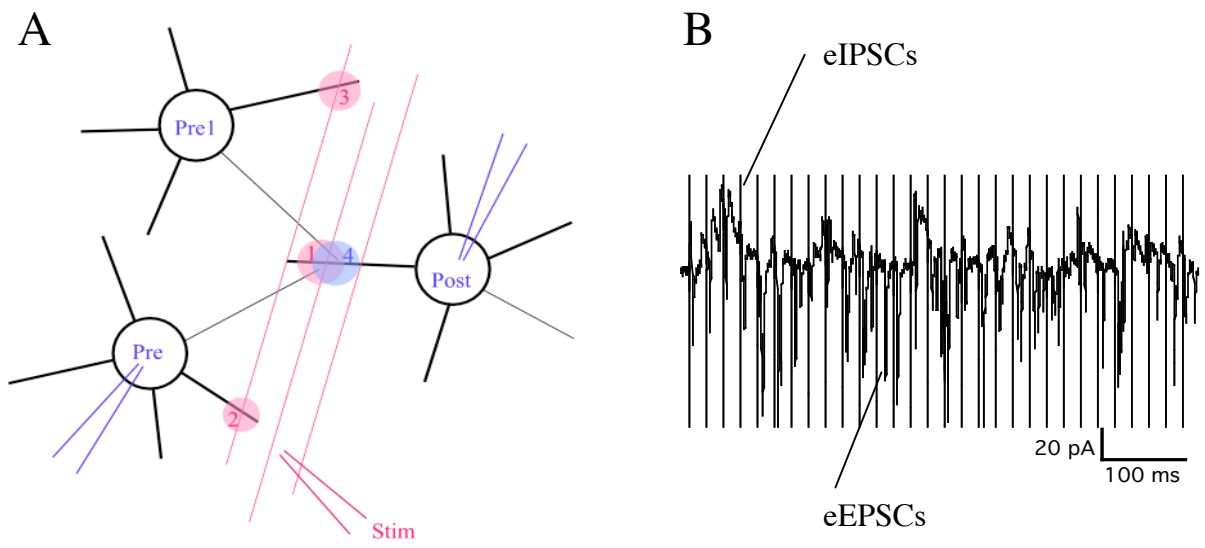

Figure 3.8 ***Glutamate and GABA spillover***

A) Schematic drawing of an interneuronal network: two synaptically connected stellate cells are patch-clamped (Pre and Post). The postsynaptic cell receives also a GABAergic input from other interneurons (e.g. Pre1). Train stimulation at parallel fibers (red lines) liberates a large amount of glutamate, which can activate axonal receptors of the presynaptic cells (circle 1). The glutamatergic input cannot activate firing in Pre because of the voltage-clamp (circle 2), but activates the not clamped cell Pre1 (circle 3). This leads to release of GABA and subsequent GABA spillover (circle 4). B) Example of postsynaptic currents recorded in the postsynaptic during train stimulation of the parallel fibers: GABAergic inhibitory currents appear as outward currents (eIPSCs) whereas glutamatergic excitatory currents are inward (eEPSCs).

In order to test the role of GABA spillover in the train stimulation induced disinhibitory effect, we affected the GABA release by acting on GABA transporters pharmacologically.
Neurotransmitter released from presynaptic axonal varicosities after vesicle exocytosis diffuses into the synaptic cleft where it activates the postsynaptic receptors, and is eventually taken up into the presynaptic cell or into neighboring glial cells by specific transporters.
At inhibitory connections between cerebellar interneurons, the reuptake of GABA into the presynaptic terminals is solely mediated by GABA transport-1 (GAT-1) (Takayama and Inoue, 2005). The GABA that is taken up into the presynapse contributes to refill the vesicles, in addition to the newly synthesized GABA in the intracellular compartments. Blocking of GAT-1 would therefore lead to a progressive decrease in the amount of GABA that can be restored into the vesicles and eventually to a reduction in the GABAergic transmission. After blockade of GAT-1 by SKF-89976A (100 μM) we observed indeed a reduction in the frequency and amplitude of spontaneous and evoked GABAergic currents recorded in stellate cells, whereas the glutamatergic transmission was not affected, as shown in the example in Fig. 3.9.

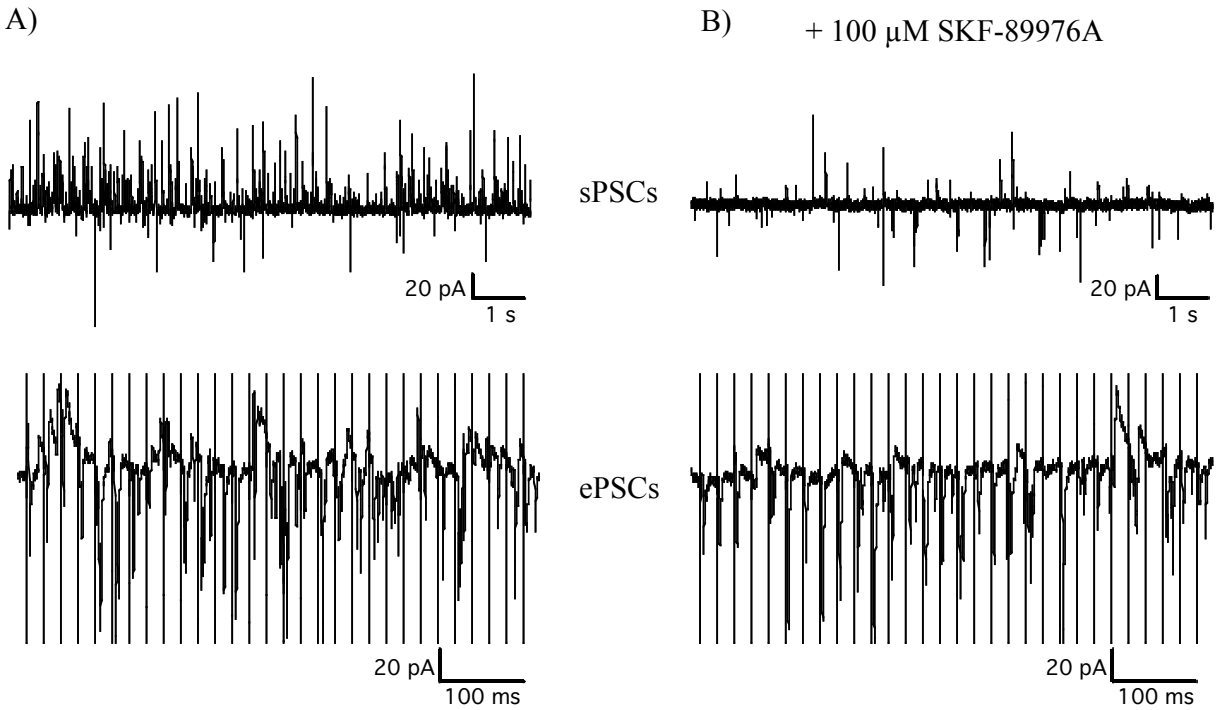

Figure 3.9 ***Blockade of neuronal GABA transporters***

Recording of spontaneous and evoked synaptic currents before (A) and after (B) blockade of GAT-1 by 100 µM SKF-89976A. Frequency and amplitude of GABAergic events (positive peaks) are reduced, whereas the glutamatergic transmission (negative peaks) is not influenced.

Blockade of GAT-1 results in a reduction of GABA spillover during the train stimulation since it limits the amount of neurotransmitter that can be released from the surrounding interneurons. We therefore checked the effect of SKF-89976A on the stimulation induced disinhibition. In these experiments, to ensure that the GABA release in the pair of interneurons examined is not influenced by GAT-1 blockade (i.e. test responses should not be affected), we added 5-10 mM GABA to the patch pipette for the presynaptic cell, which has been successfully applied in the case of glutamate in paired recordings in the hippocampus (Biro and Nusser, 2005).

The disinhibitory effect obtained with 30 stimuli at 50 Hz in the granule cell layer (32.5 ± 5.8 % reduction of eIPSCs, n = 8, $p < 0.01$) was reduced to a no longer significant level by superfusion of 100 μM SKF-89976A (12.9 ± 8.3 % reduction, $p = 0.23$) as shown in Fig. 3.10.

This result is consistent with the hypothesis the GABA spillover is also produced during train stimulation and mediates the disinhibitory effect in addition to glutamate spillover. A series of experiments was therefore performed in order to assess the type and the localization of the receptors that are activated by glutamate and GABA spillover.

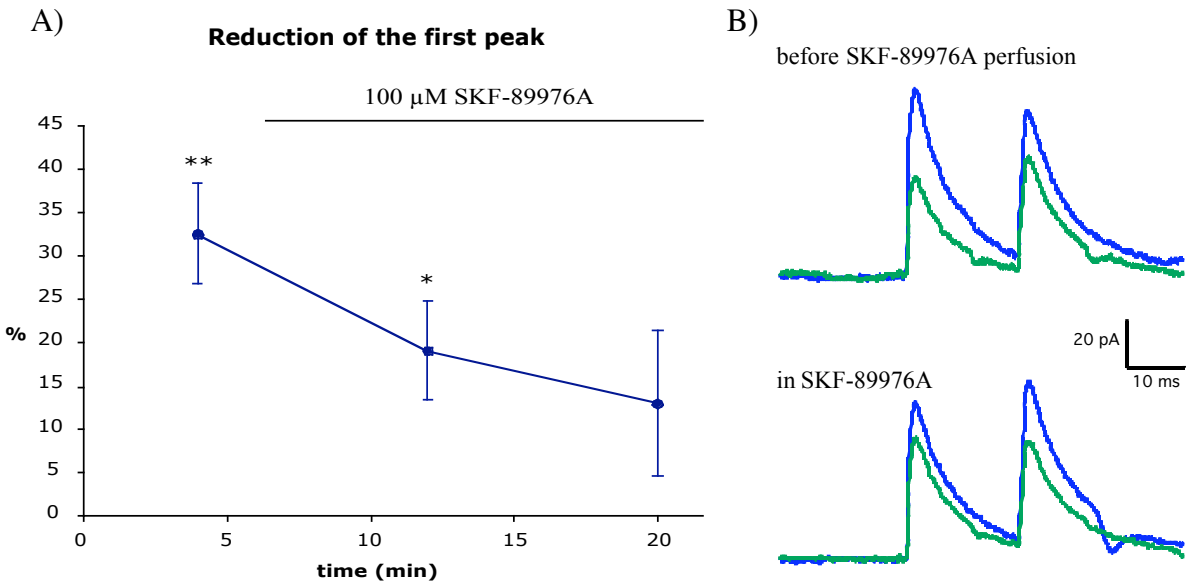

Figure 3.10 ***Effect of limited GABA spillover***

GAT-1 were blocked by addition of 100 µM SKF-89976A to the extracellular medium. A) The reduction of the first peak of conditioned responses compared to test responses is plotted against the time of presynaptic whole-cell. Each data point in the diagram corresponds to the average of 16 responses. B) Example traces from a single recording: average test responses (blue traces) and conditioned responses (green traces) before and after perfusion of the GAT-1 blocker.

3.3.1 Presynaptic $GABA_B$ receptors

Our data indicate that train stimulation in the granule cells leads to spillover of both glutamate and GABA in the molecular layer. As suggested by the experiment with the extracellular blocker CGP-55845A, $GABA_B$ receptors become activated by GABA spillover, and are responsible for almost 50% of the effect on eIPSCs. We next addressed the question, whether this receptors are localized pre- or postsynaptically.

It has recently been shown that presynaptic $GABA_B$ receptors modulate GABA release at synapses between cerebellar interneurons by inhibiting voltage dependent Ca^{2+} channels via a metabotropic pathway involving G-proteins (Mann-Metzer and Yarom, 2002). In paired recordings from connected interneurons, application of the $GABA_B$ receptor agonist baclofen (10 μM) led to a decrease in the postsynaptic response and an increase in the failure rate, which is reflected in our findings where the effect was achieved with physiological release of endogenous transmitter. Furthermore the action potential independent quantal release of GABA was profoundly depressed by baclofen.

To prove that $GABA_B$ receptors participate to the effect on eIPSCs by acting at a presynaptic site via a G-protein coupled mechanism, we included GDPβ-S in the patch pipette for the presynaptic cell to block the intracellular G-proteins. Once the whole-cell configuration is reached, the solution contained in the patch pipette dialyses the cell and the blocker diffuses in the cytoplasm within 5-10 minutes. Since a longer recording time in double patch recordings is hampered by the problem of synaptic rundown, we restricted the analysis to recordings of 15 minutes, discarded the synapses showing a decline larger than 50% in the peak amplitude of test responses, and tested two different concentrations of GDPβ-S to control the diffusion efficiency.

In the first minutes of presynaptic whole-cell recording with 1 mM GDPβ-S, a train of 30 stimuli at 50 Hz in the granule cell layer resulted in a significant disinhibition (29.1 ± 9.9 %) that linearly declined to 12.3 ± 5.2 % in the last time point (n = 8) (Fig. 3.11). With 3 mM intracellular GDPβ-S, the initial significant reduction of eIPSCs of 33.3 ± 7.3 % declined to a plateau within few minutes, reaching a final value of 16.2 ± 9.5 % in the last time point (n = 6).

This result proves the involvement of a G-protein coupled pathway in the presynaptic cell, likely initiated by presynaptic $GABA_B$ receptors activated by GABA spillover. The fact that the disinhibitory effect was not completely blocked by GDPβ-S (in both applied

concentrations) suggests the involvement of a second pathway initiated by ionotropic receptors.

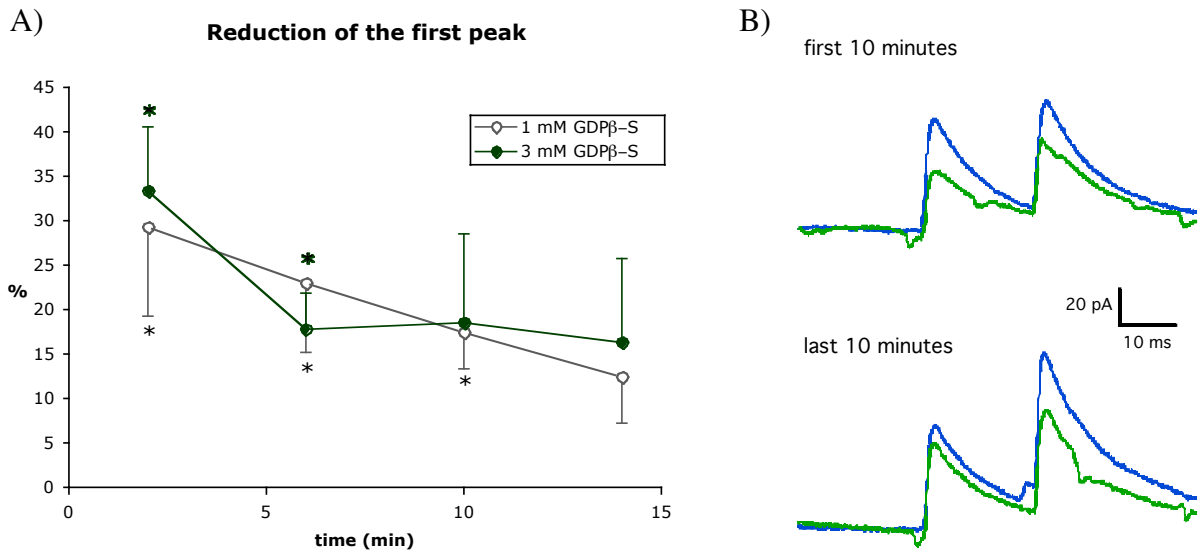

Figure 3.11 ***Blockade of intracellular G proteins***

A) Presynaptic G proteins were blocked by adding 1 mM (open circles) or 3 mM (full circles) GDPβ-S in the patch pipette for the presynaptic cell. The reduction of the first peak of conditioned responses compared to test responses is plotted against the time of presynaptic whole-cell. Each data point in the diagram corresponds to the average of 8 responses. B) Example traces from a single recording: average test responses (blue traces) and conditioned responses (green traces) during the first and the last 10 minutes of recording with 1 mM GDPβ-S in the patch pipette. The small negative peaks in the average traces arise from conditioned responses that contained EPSCs.

We next asked whether the fact that the disinhibitory effect was reduced in three-week old mice could be attributable to a developmental switch in the localization of $GABA_B$ receptors. We tested the effect of baclofen on the quantal release in P13 and P21-22 mice, as it was previously done in P7-17 Guinea pigs (Mann-Metzer and Yarom, 2002). Superfusion of 10 μM baclofen led to a significant decrease in the frequency of mIPSCs (miniature Inhibitory PostSynaptic Currents) recorded in the presence of the voltage dependent Na^+ channel blocker tetrodotoxin (TTX, 1 μM), as shown in Fig. 3.12. In P13 mice, the frequency of mIPSCs was reduced by 58.4 ± 12.5 % ($n = 5$, $p < 0.05$) with no significant change in the average peak

amplitude (data not shown). This effect persisted in P21-22 mice, where the frequency reduction was 50.9 ± 4.0 % (n = 6, $p < 0.05$). This result excludes that presynaptic $GABA_B$ receptors undergo a developmental change in the age examined in our experiments. The reduction of the disinhibitory effect is therefore not attributable to the metabotropic pathway.

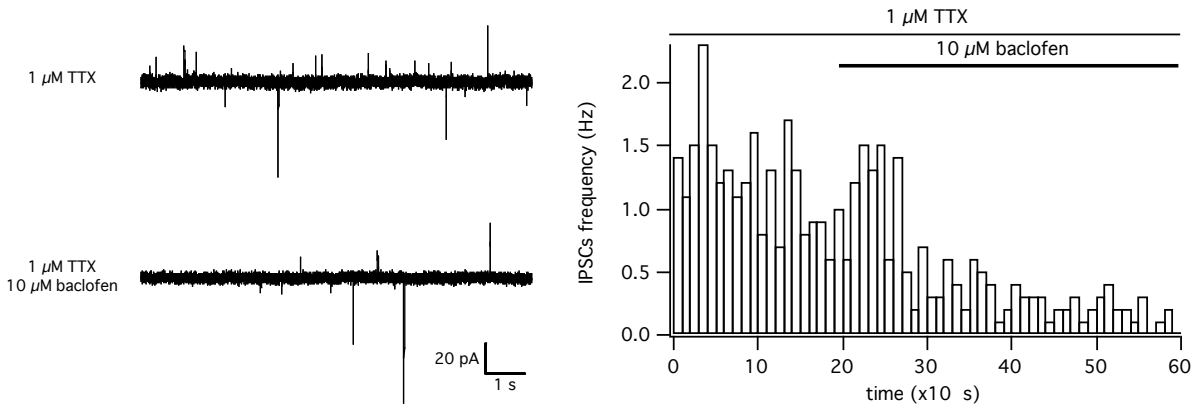

Figure 3.12 ***Presynaptic $GABA_B$ receptors affect quantal release***

Representative traces showing the recording of miniature currents in a cerebellar stellate cell from a P13 mouse in the presence of 1 μM TTX (left panel). The cell was voltage-clamped at –35 mV, in order to distinguish the outward mIPSCs from the inward mEPSCs. Perfusion of 10 μM baclofen decreased the frequency of mIPSCs, as reflected in the frequency histogram (right panel).

3.3.2 Presynaptic AMPARs

The experiments described so far provide evidence that $GABA_B$ receptors contribute in mediating the disinhibition via a metabotropic pathway involving G-proteins. Blockade of $GABA_B$ receptors with extracellular CGP-58554A resulted in a reduction of eIPSCs of 10.5 ± 4.6 %. Consistent with these observations, blockade of presynaptic G-proteins by GDPβ-S led to a disinhibitory effect between 12.3 ± 5.2 % and 16.2 ± 9.5 % depending on the concentration used.

In contrast to $GABA_B$ receptor blockers, the AMPAR selective antagonist GYKI 53655 was more efficient in suppressing the modulation of GABA release (5.1 ± 3.5 % reduction left). This suggests that the AMPARs may exert not only an indirect postsynaptic action, i.e. excitation of surrounding interneurons leading to spillover of GABA and activation of $GABA_B$ receptor in the presynaptic stellate cell, but may also act directly at the presynaptic site following glutamate spillover.

It has been previously shown (Bureau and Mulle, 1998) that AMPARs in cerebellar interneurons modulate GABAergic transmission, based on the following observations. Perfusion of AMPAR agonists led to an increase in the frequency of action potential independent quantal GABAergic events (mIPSCs) recorded in the presence of TTX. Blockade of voltage gated sodium channels by TTX prevents cell firing despite activation of postsynaptic AMPARs. Therefore, the augmented GABAergic transmission can be attributed to presynaptic AMPARs, which are located on the cell axon near to release sites. When activated by the agonist, they depolarize locally the axon, leading to gating of voltage dependent Calcium channels and subsequent enhancement in GABA release. This effect was present in two week-old mice and no longer in three week-old mice, indicating a developmental switch in AMPAR localization.

We confirmed these results in our experimental condition using Kainate (KA) as AMPAR agonist. Perfusion of 2 μM KA significantly increased the frequency of mIPSCs recorded in stellate cells from P13-15 mice from 0.88 ± 0.24 Hz to 1.54 ± 0.39 Hz ($n = 10$, $p < 0.05$), with no significant change on the average peak amplitude (data not shown). A single recording is depicted in Fig. 3.13.

It has also been shown that presynaptic AMPARs induce a reduction in action potential dependent GABA release (evoked release) at the synapse between basket cells and Purkinje cells when activated by spillover of glutamate released by climbing fibers (Satake et al., 2000). This effect seems to be mediated by metabotropic AMPARs (Satake et al, 2004) that

induce inhibition of voltage dependent Calcium channels and consequent decrease in GABA release from the basket cell (Rusakov et al., 2005).

Although our experiments at stellate-to-stellate synapses indicate that a metabotropic pathway is initiated by $GABA_B$ receptors, an additional contribution of presynaptic AMPAR receptors in mediating the disinhibition has to be considered. This would also account for the developmental change of the effect.

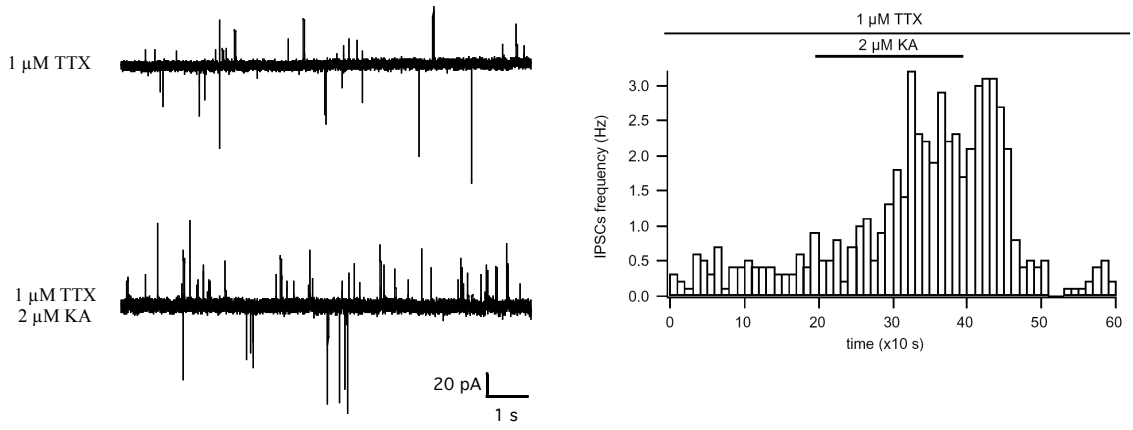

Figure 3.13 ***Presynaptic AMPARs affect quantal release***

Representative traces showing the recording of miniature currents in a cerebellar stellate cell in the presence of 1 µM TTX (left panel). The cell was voltage-clamped at –40 mV, in order to distinguish the outward mIPSCs from the inward mEPSCs. Perfusion of 2 µM KA increased the frequency of mIPSCs, as reflected in the frequency histogram (right panel).

3.4 Ca^{2+} imaging experiments from stellate cells

The experiments described so far indicate that the train stimulation-induced disinhibition at interneuronal synapses results from a reduction in the GABA release from the presynaptic cell. To reach this conclusion we analyzed the output generated in the postsynaptic cell (test and conditioned eIPSCs), which provided also information about the presynaptic site based on the analysis of failure rate, paired-pulse ratio and coefficient of variation. In the next series of experiment we focused our attention on the presynaptic site, i.e. the axon of stellate cells.

Neurotransmitter release from presynaptic terminals is triggered by Ca^{2+} influx through voltage gated Ca^{2+} channels that open when the action potential depolarizes the axonal membrane. A direct evidence for the presynaptic change underlying the disinhibitory effect can be provided by recording Ca^{2+} transients that are elicited in interneuron axons upon test and conditioned action potentials. For this aim we performed Ca^{2+} imaging experiments using Two-photon microscopy (see Methods for details about 2P microscopy).

Stellate cells were loaded with the Ca^{2+} sensitive dye Oregon Green 488 BAPTA-1 (100 μM) included in the patch pipette (Fig. 3.14). Ca^{2+} transients evoked upon firing of the cells in a double pulse paradigm (2 action currents, 20 ms interval) were recorded from regions of interest (ROIs) scanned on the axon (Fig. 3.15B). The spatial distribution of the Ca^{2+} responses along the axon confirmed the presence of "hot spots", i.e. regions where the Ca^{2+} transients show local maxima (Forti et al., 2000). These are supposed to represent functional clusters of voltage dependent Ca^{2+} channels and mostly coincide with axonal varicosities that give rise to *en passant* presynaptic sites.

We recorded test Ca^{2+} transients in hot spots from stellate cell axons and compared them with the conditioned Ca^{2+} transients elicited after train stimulation in the granule cell layer, following the protocol used for double patch experiments. For paired recordings the stimulation pipette was placed on the basis of electrophysiological responses elicited in the cell pair, whereas in Ca^{2+} imaging with single patch the monitoring of any postsynaptic cell was not performed. Furthermore, the ROIs were often chosen on regions of the axon that were distant from the dendritic region, i.e. far away from the glutamatergic postsynaptic sites, so that no electrophysiological events would be detected in the soma although neurotransmitter spillover takes place at axonal sites. To ensure that glutamate was released in a region proximal to the stellate cell axon, we traced the granule cell axons by electroporation with Alexa Fluor 594 (500 μM) contained in the stimulation pipette. Due to the electrical field generated by the stimulus, small pores are transiently produced in the membrane of granule

cells, and the charged ions of the red dye penetrate the cytoplasm and follow the driving force. A good labeling of the axon was reached after few train stimulations (Fig. 3.14).

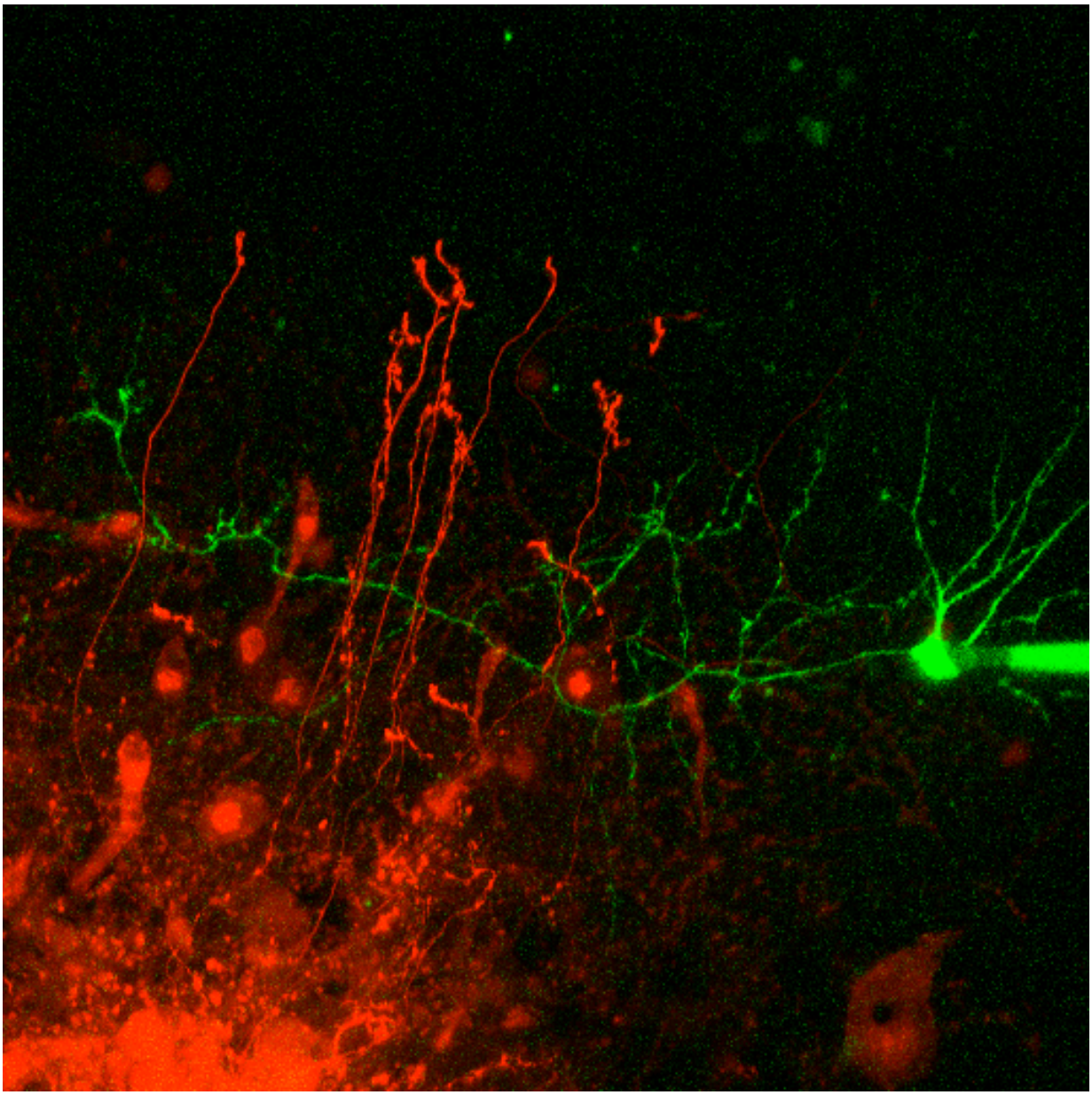

Figure 3.14 ***Loading of stellate cells and granule cells for Ca^{2+} imaging***

A stellate cell (in green) was loaded with 100 µM Oregon Green 488 BAPTA-1 contained in the patch pipette. Granule cells (in red) were filled by electroporation achieved with repetitive stimulation in the granule cell layer with an extracellular pipette containing 500 µM Alexa Fluor 594. This picture is a z-projection elaborated by collecting the maximum intensity from 28 images taken in different focal planes with 1 µm intervals. Image size: 206.8 µm x 206.8 µm.

Ca^{2+} imaging was performed in three different experimental series: in absence of drugs and in presence of either AMPA or $GABA_B$ receptor antagonists. Results from different ROIs (total number N) recorded in different cells (total number n) were analyzed as $\Delta F/F_0$, i.e. as change in the fluorescence intensity F compared to prestimulus signal F_0, as described in Methods.
The first remarkable result was that the train stimulation itself did never produce a detectable axonal Ca^{2+} signal in the tested ROIs, as shown in the example in Fig. 3.15. This excludes that a detectable Ca^{2+} influx in the axon through Ca^{2+} permeable AMPARs and/or voltage gated Ca^{2+} channels is produced by neurotransmitter spillover.

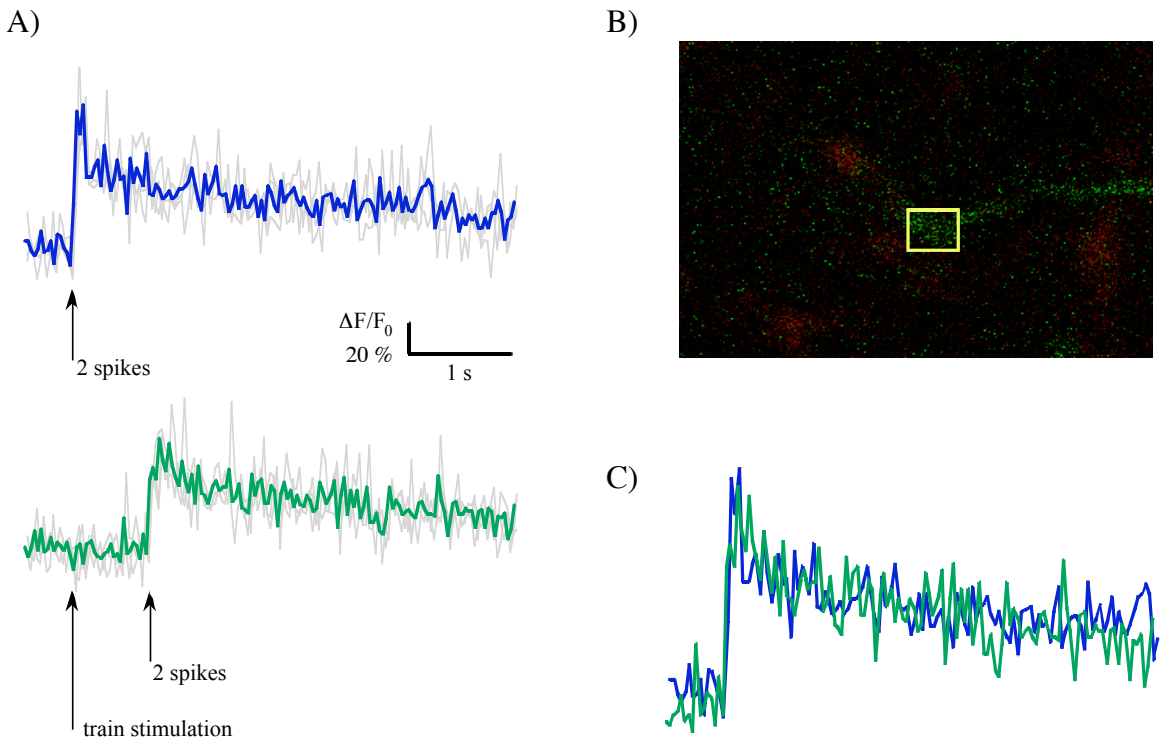

Figure 3.15 ***Axonal Ca^{2+} transients in stellate cells***

A) Ca^{2+} signals were evoked by paired-pulse spiking of the stellate cells and measured in a ROI set on the axon near to granule cell axons, as depicted in B) (image size: 40 µm x 30 µm). 3 trials for test responses and conditioned responses (gray traces) were analyzed as $\Delta F/F_0$ and averaged (blue and green trace, respectively). No Ca^{2+} signals were detected upon train stimulation. C) Scaling of the average traces revealed no change in the kinetics.

We next compared the peak amplitude of conditioned responses and compared them to test responses, as shown in Fig. 3.16 where the values indicating the relative reduction are plotted. In control experiments the average peak amplitude of conditioned Ca^{2+} transients was reduced by 11.4 ± 1.9 % (N = 53, n =9). In presence of 50 μM GYKI 53655 there was no difference between test and conditioned responses (0.15 ± 1.98 %; N = 42, n = 8). In presence of 500 nM CGP-55845A the reduction was 6.8 ± 1.6 % (N = 41, n = 8). ANOVA test revealed that the result with AMPAR blocker was significantly different from control series and experiments with $GABA_BR$ blocker ($p < 0.01$ and $p < 0.05$, respectively). No significant change in the kinetics of the Ca^{2+} transients was found in any series, as shown in the example ROI in Fig. 3.15C.

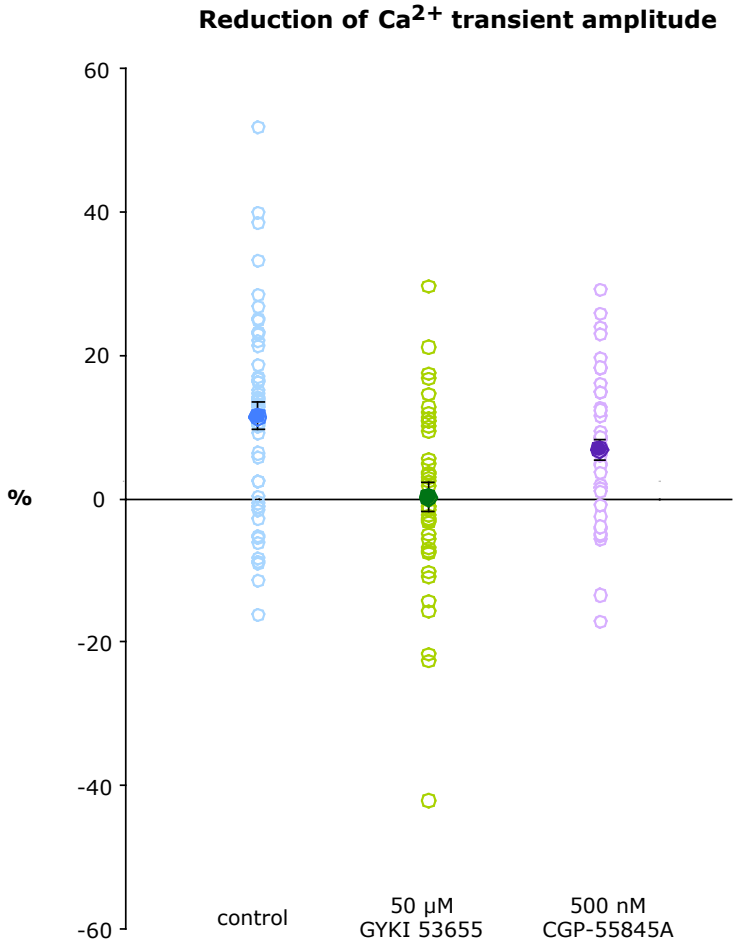

Figure 3.16 ***Reduction of axonal Ca^{2+} signals***

Reduction of the peak amplitude of conditioned Ca^{2+}transients compared to test transients were examined in all recorded ROIs (open circles) in the absence of drugs (control) and in the presence of AMPAR blocker (50 µM GYKI 53655) or $GABA_B$ receptor blocker (500 nM CGP-55485A). Mean values ± S.E.M. of each series are shown by full circles.

4. DISCUSSION

4.1 Disinhibition at stellate-to-stellate synapses via sustained parallel fiber activity

Enhanced glutamate release in the molecular layer generated by train stimulation of granule cells reduces GABA release in the stellate cell network. Amplitudes of eIPSCs elicited in pairs of synaptically connected interneurons were decreased when preceded by a conditioning train of stimuli applied in the granule cell layer. The net effect of sustained glutamate release was *disinhibition* of the interneuronal network. The effect occured within a time window of tens of milliseconds after the end of the train (up to 1 second), suggesting that the underlying mechanisms were triggered during or directly after the train and that the basal level of GABAergic transmission was restored after tens of seconds.

Surprisingly, boosting the glutamate release from granule cells, by applying a train of 60 stimuli instead of 30, resulted in a smaller reduction of eIPSCs (18% instead of 28%). Preventing AMPAR desensitization with Cyclothiazide enhanced the effect obtained with 60 stimuli (35% reduction), indicating that disinhibition does not only depend on the amount of glutamate released in the molecular layer but can be influenced by the responsiveness of AMPARs to the neurotransmitter. This interplay of pre- and postsynaptic activity may become crucial in vivo. In order to perform paired recordings from connected stellate cells in vitro, acute slices have to be prepared by cutting the cerebellum in the sagittal plane. In this way the axons of the interneurons are preserved, but the parallel fibers, i.e. the prolongation of the granule cell axons, are rather truncated, since they develop in the transverse plane. It has therefore to be considered that the amount of glutamate released upon train stimulation of granule cells in vitro might be only a fraction of that released in vivo, where the parallel fibers are intact. Hence, in vivo the disinhibition may be more pronounced even with short burst activity of granule cells (Chadderton et al., 2004).

The concomitant increase in failure rate, paired-pulse ratio and CV indicates a presynaptic expression of the effect. This may occur by a change in the release probability for GABA (p) or in the number of release sites (n), whereas the postsynaptic response to a given quantum of GABA (q) is not modified. The temporal course of the disinhibition and the fact that the basal GABAergic transmission was restored after a time period in the range of seconds (short term plasticity) indicates a change in p, since modifications in n are likely to occur on a longer time scale (long term plasticity). Further evidence for a change in p was provided by the fact that presynaptic receptors (see below) act on voltage gated Ca^{2+} channels in the axon terminal,

modifying the Ca^{2+} concentration that triggers vesicle fusion, thus affecting release probability.

4.2 Mechanisms underlying the disinhibition: AMPA and $GABA_B$ receptors

Pharmacological dissection of the disinhibitory effect provided the evidence for the involvement of two receptor types. In presence of the specific AMPAR blocker GYKI 53655, the reduction of eIPSCs was almost abolished. In presence of the $GABA_BR$ antagonist CGP-55845A the effect was partially but significantly decreased in comparison to control experiments. A metabotropic pathway was also confirmed by experiments in which the presynaptic G-proteins were blocked by intracellular GDPβ-S.

Based on these results we propose that sustained granule cell activity initiates at interneuronal synapses an action involving both ionotropic and metabotropic mechanisms via presynaptic AMPA and $GABA_B$ receptors, respectively, as synthesized in the model in Fig. 4.1. Facilitated glutamate release in the molecular layer induces firing of surrounding stellate cells. The following accumulation of GABA activates presynaptic $GABA_B$ receptors, which then inhibit voltage-gated Ca^{2+} channels via a G-protein coupled mechanism, as previously described (Mann-Metzer and Yarom, 2002). In addition to this, glutamate diffuses by spillover to the axon of stellate cells where it activates presynaptic AMPARs (Bureau and Mulle, 1998).

The final effect of AMPAR and $GABA_B$ receptors at the presynaptic site is the reduction of Ca^{2+} influx through voltage-gated Ca^{2+} channels, which lowers GABA release probability. This conclusion was supported by the results obtained with Ca^{2+} imaging experiments. Peak amplitudes of axonal Ca^{2+} transients elicited by firing of stellate cells were reduced when preceded by a conditioning train stimulation that released glutamate in a region proximal to the interneuron axon. This effect was decreased in presence of CGP-55485A and abolished by GYKI 53655, confirming that both $GABA_B$ and AMPARs act on the presynaptic site inhibiting the Ca^{2+} influx that triggers GABA release.

In has to be considered that the approach used for the imaging experiments might lead to an underestimation of the disinhibitory effect on Ca^{2+} signaling. Although the labeling of granule cell axons by electroporation with the red dye provided an indication about the proximity of the excitatory inputs to the imaged axon of the stellate cells, the amount and the spatial extension of glutamate and GABA spillover during the train stimulation could not be controlled. In addition to this, although the ROIs were chosen in correspondence to hot spots

of Ca^{2+} responses, which almost coincide with the GABA release sites (Forti et al., 2000), it could not be discriminated between the postsynaptic targets of those presynaptic terminals (interneurons or Purkinje cells). Target specificity of the disinhibitory effect would be therefore overlooked by this approach. These considerations may account for the variability found in conditioned Ca^{2+} responses (Fig. 3.16) and the lack of statistical significance in the difference between control and $GABA_BR$ blocker series. Nevertheless the average values showed a trend reflecting the electrophysiological results.

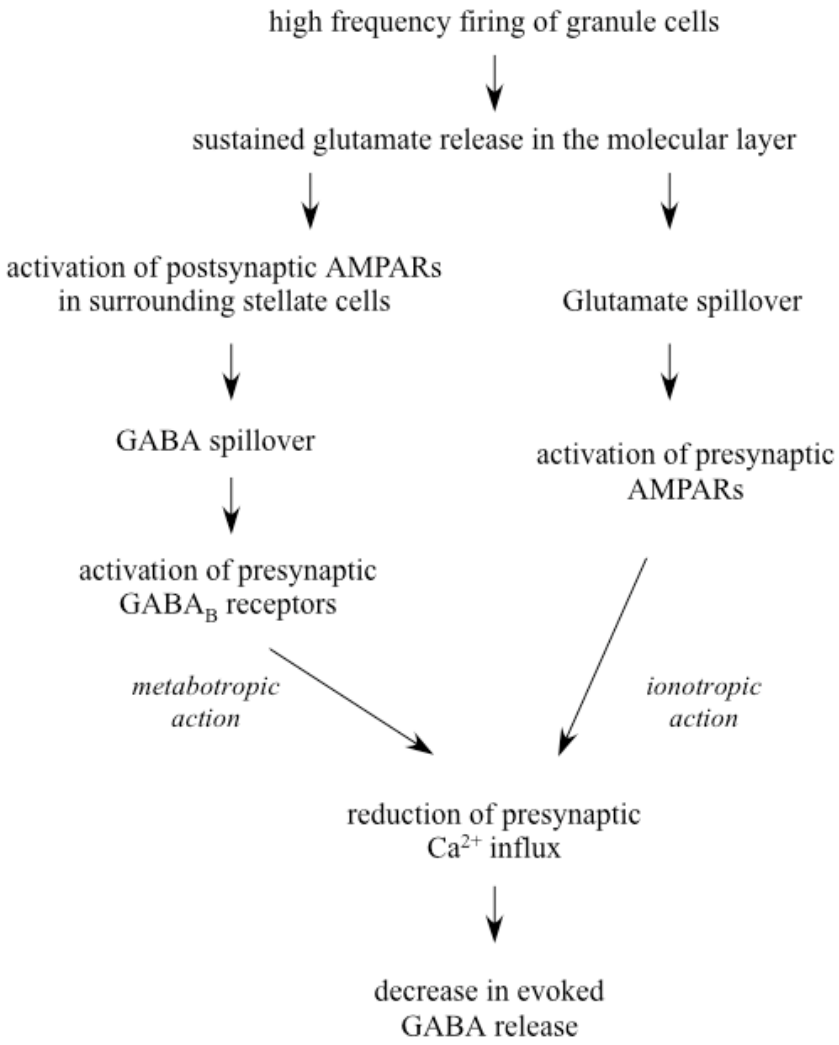

Figure 4.1 ***Model for train stimulation induced disinhibition***

4.2.1 GABA spillover: activation of presynaptic $GABA_B$ receptors

The metabotropic action of $GABA_B$ receptors in different brain regions is well known: at presynaptic sites they inhibit voltage gated Ca^{2+} channels, whereas at postsynaptic sites they activate K^+ conductance, lowering cell excitability (Misgeld et al., 1995; Yamada et al. 1999). These pre- and postsynaptic effects of $GABA_B$ receptors have been demonstrated also in cerebellar stellate cells (Mann-Metzer and Yarom, 2002).

In our experimental condition, the excitability of the presynaptic cell was controlled by the voltage clamp and only presynaptic $GABA_B$ receptors can account for a modulation of GABAergic transmission.

Whereas glutamate spillover upon high frequency firing of granule cells is conceivable (Atluri and Regehr, 1996, 1998), it needed to be tested whether the accumulation of GABA released from the surrounding stellate cells during the train stimulation could be responsible for the activation of $GABA_B$ receptors. For this purpose we blocked the reuptake of GABA into the presynaptic vesicles with a GAT-1 inhibitor, which led to a progressive reduction of the inhibitory responses during the train. Importantly, the basal GABAergic transmission between the cell pairs under patch condition was kept constant by adding GABA to the patch pipette for the presynaptic cell. With this approach the disinhibitory effect was reduced to a similar extent as with $GABA_B$ receptor and G-protein blockers, confirming the role of GABA spillover in activating the metabotropic pathway.

4.2.2 Glutamate spillover: activation of presynaptic AMPA receptors

The involvement of presynaptic AMPARs is indicated by the fact that in both paired-recording and Ca^{2+} imaging experiments the disinhibitory effect was suppressed by the AMPAR selective antagonist, whereas the blockade of the metabotropic pathway produced only a partial reduction. Hence, besides the postsynaptic action that induces firing of surrounding stellate cells and consequent GABA spillover activating metabotropic receptors, a direct involvement of AMPARs is conceivable. Since the features of the effect indicate a presynaptic site of expression, the AMPARs must be localized in the presynaptic cell. Due to the whole-cell condition during double patch recordings, activation of dendritic AMPARs in the presynaptic cell can unlikely affect the axonal sites, since any dendritic signal generated by the train would be blocked in the soma by the voltage-clamp to –60 mV. Thus, one has to consider presynaptic AMPARs, localized in the axonal compartments of the cell.

Evidence has recently accumulated showing that AMPARs, in addition to their classical postsynaptic localization, can also be found at presynaptic sites. AMPAR subunits have been detected in presynaptic terminals of the hippocampus, dorsal root ganglia and cerebellar interneurons (Fabian-Fine et al., 2000; Lee et al., 2002; Lu et al., 2002; Schenk et al., 2003; Satake et al., 2006).

A detailed characterization of presynaptic AMPARs has been carried out at the synapse between basket cell and Purkinje cell in the molecular layer of the cerebellum. Spillover of glutamate from the climbing fibers was found to activate AMPARs in the terminals of basket cells leading to a reduction of GABA release (Satake et al., 2000). This effect was supposed to involve a G-protein dependent pathway initiated by AMPARs, resulting in inhibition of presynaptic Ca^{2+} channels (Satake et al., 2004; Rusakov et al., 2005). Further studies indicated a crucial role of AMPARs containing the GluR-B subunit, which confers Ca^{2+} impermeability to the channels (Satake et al., 2006).

These findings supported the hypothesis that AMPARs may also possess metabotropic properties (Wang et al., 1997), independent of the ligand gated ion influx, which is the main feature of ionotropic channels. Further evidence for a G-protein coupled function has been provided by a study at the calyx of Held (Takago et al., 2005), where presynaptic AMPARs also mediate inhibition of transmitter release.

Nevertheless the existence of metabotropic functions for AMPARs remains a matter of debate: many studies were performed using high concentration of exogenous agonists, which might not reflect physiological conditions, and little information is available about the identity of the cellular compartment where AMPARs couple to biochemical signal cascades (Schenk and Matteoli, 2004). Furthermore, the properties of presynaptic AMPARs could be different at different synapses. In dorsal root neurons, for example, presynaptic AMPARs are supposed to inhibit neurotransmitter release via pure ionotropic mechanisms (Lee et al., 2002; Engelman et al., 2006).

In cerebellar stellate cells the presence of presynaptic AMPARs has been postulated to explain the positive regulating effect of AMPAR agonists on the action potential independent GABA release (Bureau and Mulle, 1998). Here, we studied the effect of endogenously released glutamate on action potential dependent GABA release. Our results from paired recordings and Ca^{2+} imaging indicate that presynaptic AMPARs concur with $GABA_B$ receptors in decreasing GABA release by inhibiting Ca^{2+} signaling (in two week-old mice, see below). The opposite effects of presynaptic AMPARs on spontaneous and evoked release (mIPSCs are enhanced whereas eIPSCs are depressed) have been reported for a number of

presynaptic receptors including NMDARs in cerebellar interneurons (Glitsch and Marty, 1999) and AMPARs and in the dorsal horn (Engelman et al., 2006). This discrepancy may arise from the different mechanisms underlying neurotransmitter release and from the experimental approaches used to activate the presynaptic receptors. For studying effects on quantal release, iGluRs have to be activated by prolonged application of exogenous agonists. This may produce a long lasting depolarization of the axon terminal, which induces a progressive accumulation of Ca^{2+}, resulting in enhanced spontaneous release. When examining evoked release, like in our paired recordings, gating of ionotropic receptors can be achieved by release of endogenous glutamate. In this case the neurotransmitter is only present for a short time, as is characteristic for physiological synaptic transmission. If presynaptic iGluRs are activated by glutamate spillover, the conductance of the axonal membrane is transiently altered. This causes shunting of incoming action potentials that are reduced in amplitude and activate voltage dependent Ca^{2+} channels to a lower extent.

Although more experiments are needed to confirm this hypothesis, our data strongly indicate that presynaptic AMPARs in stellate cells exert a pure ionotropic action on evoked release, as described above, and that the metabotropic feature of the disinhibitory effect is only attributable to $GABA_B$ receptors. This implies a difference between the two types of molecular layer interneurons. At basket cell-to-Purkinje cell synapses the suppression of GABA release triggered by climbing fiber activation is likely modulated by metabotropic AMPARs, in particular by Ca^{2+} impermeable AMPARs (containing the GluR-B subunit), without involvement of $GABA_B$ receptors (Satake et al, 2000, 2004, 2006). At stellate cell-to-stellate cell synapses both AMPARs and $GABA_B$ receptors can mediate disinhibition and AMPARs act via ionotropic mechanisms. Furthermore, the effect does not depend on the GluR-B subunit, since disinhibition was inducible in knock-out mice that lack this subunit (GluR-$B^{-/-}$) (data not shown).

As a final remark, one should add that a definitive proof for the involvement of presynaptic AMPARs in modulating evoked GABA release would be provided if it were possible to block specifically the AMPARs in the presynaptic cell with an intracellular blocker (as in the case of GDPβ-S for the G-proteins). This would not interfere with the activity in the surrounding molecular layer, leaving unaffected the GABA spillover induced by train stimulation, whereas application of extracellular antagonists, such as GYKI 53655, blocks all AMPARs of the circuit and all possible downstream signaling. Since a blocker acting on the intracellular

domain of AMPARs is not available, only indirect evidence for the involvement of these receptors at presynaptic sites could be provided.

4.3 Developmental regulation

The train stimulation-mediated disinhibition in the stellate cell network was developmentally regulated. Conditioned eIPSCs were consistently more affected in two week-old mice than in three week-old mice. Limitations in neurotransmitter spillover due to an improved glutamate uptake system did not account for this difference, which persisted although glutamate transporters were inhibited by TBOA in slices from P18-22 mice.

An age dependent modification in the expression of presynaptic receptors provides an explanation to this issue.

It has been previously suggested that AMPARs are localized only transiently in the axon of stellate cells (Bureau and Mulle, 1998). The AMPAR mediated effect on quantal release of GABA was inducible in P13-15 but no longer in P21-25 mice.

To test whether also presynaptic $GABA_B$ receptors undergo a similar switch, we examined the effect of their agonist on quantal release. Application of baclofen increased the frequency of mIPSCs in two week-old mice, and this effect was unaltered in three week-old animals. This excludes an age dependent regulation of $GABA_B$ receptors.

Based on these findings, we conclude that presynaptic $GABA_B$ receptors mediate the spillover induced disinhibition at all examined developmental stages, and that in two week-old mice this effect is strengthened by the concomitant activation of presynaptic AMPARs.

4.4 Physiological relevance

The disinhibitory effect on GABAergic transmission between stellate cells represents a further example of neurotransmitter spillover mediated transmission, which enriches the features of chemical signaling at central synapses (Huang, 1998). Due to sustained activity of granule cells and interneurons, glutamate and GABA molecules accumulate and diffuse to nearby synapses, where they can activate presynaptic receptors. Furthermore, the negative regulation of inhibitory synapses triggered by excitatory inputs constitutes a form of heterosynaptic depression, which seems to be a characteristic of the cerebellar circuitry (Satake et al., 2000).

Sustained glutamate release from parallel fibers has physiological relevance during perception, since it has been shown in vivo that somatosensory stimulation generates bursts of spikes in granule cells (Chadderton et al., 2004). Furthermore, in vitro studies have

demonstrated that train stimulation paradigms induce forms of long term plasticity at excitatory synapses between parallel fibers and interneurons (Smith and Otis, 2005; Soler-Llavina and Sabatini, 2006).

During the induction of these plasticity paradigms, disinhibition of GABAergic transmission could play an important role by modifying the balance between inhibitory and excitatory inputs in the molecular layer. Thus, the disinhibitory effect that acts on GABAergic synapses between interneurons, with a temporal profile characteristic for short term plasticity, could affect excitatory synapses between parallel fibers and interneurons within a longer time scale. The age dependence of the effect suggests that this mechanism could be critical in early stages of development when plastic changes are crucial for the refinement of synaptic connections and for the maturation of the cerebellar circuitry.

4.5 Concluding remarks

Using two different experimental approaches we demonstrated that inhibitory transmission between cerebellar stellate cells is regulated by sustained excitatory inputs by means of neurotransmitter spillover and cross talk phenomena. Double patch recordings from connected interneurons allowed us to study the functional properties of this effect at the single synapse level and provided evidence for a presynaptic site of expression. Results obtained with Ca^{2+} imaging experiments supported this view. In both experimental series, pharmacological tools indicated a concomitant involvement of ionotropic and metabotropic presynaptic receptors.

Importantly, these results were obtained using a paradigm that reproduced physiological conditions, since the disinhibitory effect was evoked by endogenous transmitter release within a stimulation protocol that resembles activity patterns occurring in vivo, and not by perfusion of exogenous agonists. These considerations indicate the physiological relevance of the effect and provide the basis for further investigations.

5. ABBREVIATIONS

A	Ampere
ACSF	artificial cerebrospinal fluid
AIDA	(RS)-1-aminoindan-1,5-dicarboxylic acid
AM251	N-(piperidin-1-yl)-5-(4-iodophenyl)-1-(2,4-dichlorophenyl)-4-methyl-1H-pyrazole-3-carboxamide
AMPA	L-α-amino-3-hydroxy-5-methyl-4-isoxazolepropionic acid
AMPAR	AMPA receptor
ANOVA	analysis of variance
APV	D-5-amino phosphonate pentanoic acid
ATP	adenosine triphosphate
Baclofen	4-Amino-3-(4-chlorophenyl)butanoic acid
B	background intensity
BAPTA	1,2-bis(2-aminophenoxy)ethane-N,N,N',N'-tetraacetic acid
C	Coulomb or capacitance
CB	cannabinoid
CGP	(2*S*)-3-[(1*S*)-1-(3,4-dichlorophenyl)ethyl]amino-2 hydroxypropyl (phenylmethyl)phosphinic acid
CNS	central nervous system
CPPG	(RS)-α-cyclopropyl-4-phosphonophenylglycine
CV	coefficient of variation
CTZ	cyclothiyazide
EGTA	ethylene glycol-bis(2-aminoethyl)-N,N,N',N'-tetraacetic acid
EPSC	excitatory postsynaptic current
EPSP	excitatory postsynaptic potential
et al.	et alii
F	Farad or fluorescence intensity
Fig.	figure
g	conductance
G-protein	guanosine nucleotide-binding protein
GABA	γ-Aminobutyric acid
GAT	GABA transporter

GC	granule cell
GluR	glutamate receptor
GTP	guanosine triphosphate
GDPβ-S	guanosine 5'-[beta-thio]diphosphate
GYKI	1-(4-aminophenyl)-3-methylcarbamoyl-4-methyl-3,4-dihydro-7,8-methylenedioxy- 5H-2,3-benzodiazepine
HEPES	N-(2-hydroxyethyl)piperazine-N'-ethanesulfonic acid
Hz	Hertz
I	current intensity
i.e.	id est
iGluR	ionotropic glutamate receptor
IPSC	inhibitory postsynaptic current
IPSP	inhibitory postsynaptic potential
J	Joule
k	kilo
K	Kelvin
KA	kainate
l	liter
LTD	long term depression
LTP	long term potentiation
μ	micro
m	meter, milli or miniature
M	Mol or Mega
(S)-MCPG	(S)-α-methyl-4-carboxyphenylglycine
mGluR	metabotropic glutamate receptor
ML	molecular layer
mOsM	milliosmol
n	nano
n	number (of experiments)
NMDA	N-methyl-D-aspartate
NMDAR	NMDA receptor
Ω	Ohm
Osm	Osmol

p	pico
p	probability
P	postnatal
PC	Purkinje cell
QX-314	N-(2,6-dimethylphenylcarbamoylmethyl) triethylammonium
R	resistance
ROI	region of interest
s	second
S	Siemens
SEM	standard error of the mean
SKF	1-(4,4-diphenyl-3-butenyl)-3-piperidinecarboxylic acid
t	time
TBOA	DL-threo-β-benzyloxyaspartic acid
TTX	tetrodotoxin
V	Volts
2PE	Two-photon Excitation

6. REFERENCES

Atluri PP, Regehr WG (1996) Determinants of the time course of facilitation at the granule cell to Purkinje cell synapse. J Neurosci 16:5661-5671.

Atluri PP, Regehr WG (1998) Delayed release of neurotransmitter from cerebellar granule cells. J Neurosci 18:8214-8227.

Barbour B, Keller BU, Llano I, Marty A (1994) Prolonged presence of glutamate during excitatory synaptic transmission to cerebellar Purkinje cells. Neuron 12:1331-1343.

Bekkers JM (1994) Quantal analysis of synaptic transmission in the central nervous system. Curr Opin Neurobiol 4:360-365.

Bekkers JM, Stevens CF (1996) Cable properties of cultured hippocampal neurons determined from sucrose-evoked miniature EPSCs. J Neurophysiol 75:1250-1255.

Bennett MV (1997) Gap junctions as electrical synapses. J Neurocytol 26:349-366.

Betz WJ (1970) Depression of transmitter release at the neuromuscular junction of the frog. J Physiol 206:629-644.

Biro AA, Nusser Z (2005) Synapse independence breaks down during highly synchronous network activity in the rat hippocampus. Eur J Neurosci 22:1257-1262.

Bliss TV, Lomo T (1970) Plasticity in a monosynaptic cortical pathway. J Physiol 207:61P.

Bliss TV, Collingridge GL (1993) A synaptic model of memory: long-term potentiation in the hippocampus. Nature 361:31-39.

Brenner HR, Sakmann B (1978) Gating properties of acetycholine receptor in newly formed neuromuscular synapses. Nature 271:366-368.

Bureau I, Mulle C (1998) Potentiation of GABAergic synaptic transmission by AMPA receptors in mouse cerebellar stellate cells: changes during development. J Physiol 509 (Pt 3):817-831.

Cajal SRY (1894) La Fine Structure des Centres Nerveux. Proc R Soc Lond 55:444-468.

Carter AG, Regehr WG (2000) Prolonged synaptic currents and glutamate spillover at the parallel fiber to stellate cell synapse. J Neurosci 20:4423-4434.

Castillo J, Katz B (1954) Quantal components of the end-plate potential. J Physiol 124:560-573.

Centonze VE, White JG (1998) Multiphoton excitation provides optical sections from deeper within scattering specimens than confocal imaging. Biophys J 75:2015-2024.

Chadderton P, Margrie TW, Hausser M (2004) Integration of quanta in cerebellar granule cells during sensory processing. Nature 428:856-860.

Chavas J, Marty A (2003) Coexistence of excitatory and inhibitory GABA synapses in the cerebellar interneuron network. J Neurosci 23:2019-2031.

Clark BA, Cull-Candy SG (2002) Activity-dependent recruitment of extrasynaptic NMDA receptor activation at an AMPA receptor-only synapse. J Neurosci 22:4428-4436.

Conchello JA, Lichtman JW (2005) Optical sectioning microscopy. Nat Methods 2:920-931.

Crair MC, Malenka RC (1995) A critical period for long-term potentiation at thalamocortical synapses. Nature 375:325-328.

Denk W (1994) Two-photon scanning photochemical microscopy: mapping ligand-gated ion channel distributions. Proc Natl Acad Sci U S A 91:6629-6633.

Denk W, Svoboda K (1997) Photon upmanship: why multiphoton imaging is more than a gimmick. Neuron 18:351-357.

Denk W, Strickler JH, Webb WW (1990) Two-photon laser scanning fluorescence microscopy. Science 248:73-76.

Diana MA, Marty A (2003) Characterization of depolarization-induced suppression of inhibition using paired interneuron--Purkinje cell recordings. J Neurosci 23:5906-5918.

Diana MA, Bregestovski P (2005) Calcium and endocannabinoids in the modulation of inhibitory synaptic transmission. Cell Calcium 37:497-505.

Egertova M, Giang DK, Cravatt BF, Elphick MR (1998) A new perspective on cannabinoid signalling: complementary localization of fatty acid amide hydrolase and the CB1 receptor in rat brain. Proc Biol Sci 265:2081-2085.

Engelman HS, Anderson RL, Daniele C, Macdermott AB (2006) Presynaptic alpha-amino-3-hydroxy-5-methyl-4-isoxazolepropionic acid (AMPA) receptors modulate release of inhibitory amino acids in rat spinal cord dorsal horn. Neuroscience 139:539-553.

Faber DS, Korn H (1991) Applicability of the coefficient of variation method for analyzing synaptic plasticity. Biophys J 60:1288-1294.

Fabian-Fine R, Volknandt W, Fine A, Stewart MG (2000) Age-dependent pre- and postsynaptic distribution of AMPA receptors at synapses in CA3 stratum radiatum of hippocampal slice cultures compared with intact brain. Eur J Neurosci 12:3687-3700.

Fields RD, Stevens-Graham B (2002) New insights into neuron-glia communication. Science 298:556-562.

Forti L, Pouzat C, Llano I (2000) Action potential-evoked Ca^{2+} signals and calcium channels in axons of developing rat cerebellar interneurones. J Physiol 527 Pt 1:33-48.

Galarreta M, Hestrin S (2001) Electrical synapses between GABA-releasing interneurons. Nat Rev Neurosci 2:425-433.

Glitsch M, Marty A (1999) Presynaptic effects of NMDA in cerebellar Purkinje cells and interneurons. J Neurosci 19:511-519.

Göppert-Mayer, M. (1931) Über Elementarakte mit zwei Quantensprüngen. Annalen der Physik 9:273.

Grosche J, Kettenmann H, Reichenbach A (2002) Bergmann glial cells form distinct morphological structures to interact with cerebellar neurons. J Neurosci Res 68:138-149.

Hamill OP, Marty A, Neher E, Sakmann B, Sigworth FJ (1981) Improved patch-clamp techniques for high-resolution current recording from cells and cell-free membrane patches. Pflugers Arch 391:85-

100.

Hausser M (2001) Synaptic function: dendritic democracy. Curr Biol 11:R10-12.

Helmchen F, Denk W (2005) Deep tissue two-photon microscopy. Nat Methods 2:932-940.

Hodgkin AL, Huxley AF (1952) Propagation of electrical signals along giant nerve fibers. Proc R Soc Lond B Biol Sci 140:177-183.

Huang EP (1998) Synaptic transmission: spillover at central synapses. Curr Biol 8:R613-615.

Husi H, Ward MA, Choudhary JS, Blackstock WP, Grant SG (2000) Proteomic analysis of NMDA receptor-adhesion protein signaling complexes. Nat Neurosci 3:661-669.

Isaac JT, Nicoll RA, Malenka RC (1995) Evidence for silent synapses: implications for the expression of LTP. Neuron 15:427-434.

Kandel ER, Schwartz JH, Jessel TM (2000) Principles of Neural Science. Fourth edition. Elsevier Science Publishing.

Katz B, Miledi R (1968) The role of calcium in neuromuscular facilitation. J Physiol 195:481-492.

Kleinfeld D, Mitra PP, Helmchen F, Denk W (1998) Fluctuations and stimulus-induced changes in blood flow observed in individual capillaries in layers 2 through 4 of rat neocortex. Proc Natl Acad Sci U S A 95:15741-15746.

Koester HJ, Sakmann B (1998) Calcium dynamics in single spines during coincident pre- and postsynaptic activity depend on relative timing of back-propagating action potentials and subthreshold excitatory postsynaptic potentials. Proc Natl Acad Sci U S A 95:9596-9601.

Kondo S, Marty A (1998) Synaptic currents at individual connections among stellate cells in rat cerebellar slices. J Physiol 509 (Pt 1):221-232.

Kullmann DM, Erdemli G, Asztely F (1996) LTP of AMPA and NMDA receptor-mediated signals: evidence for presynaptic expression and extrasynaptic glutamate spill-over. Neuron 17:461-474.

Lee CJ, Bardoni R, Tong CK, Engelman HS, Joseph DJ, Magherini PC, MacDermott AB (2002) Functional expression of AMPA receptors on central terminals of rat dorsal root ganglion neurons and presynaptic inhibition of glutamate release. Neuron 35:135-146.

Lichtman JW, Magrassi L, Purves D (1987) Visualization of neuromuscular junctions over periods of several months in living mice. J Neurosci 7:1215-1222.

Llano I, Gerschenfeld HM (1993) Inhibitory synaptic currents in stellate cells of rat cerebellar slices. J Physiol 468:177-200.

Llano I, Marty A (1995) Presynaptic metabotropic glutamatergic regulation of inhibitory synapses in rat cerebellar slices. J Physiol 486 (Pt 1):163-176.

Lu CR, Hwang SJ, Phend KD, Rustioni A, Valtschanoff JG (2002) Primary afferent terminals in spinal cord express presynaptic AMPA receptors. J Neurosci 22:9522-9529.

Luscher C, Nicoll RA, Malenka RC, Muller D (2000) Synaptic plasticity and dynamic modulation of the postsynaptic membrane. Nat Neurosci 3:545-550.

Malinow R, Mainen ZF, Hayashi Y (2000) LTP mechanisms: from silence to four-lane traffic. Curr Opin Neurobiol 10:352-357.

Mann-Metzer P, Yarom Y (2002) Pre- and postsynaptic inhibition mediated by GABA(B) receptors in cerebellar inhibitory interneurons. J Neurophysiol 87:183-190.

Markram H, Tsodyks M (1996) Redistribution of synaptic efficacy between neocortical pyramidal neurons. Nature 382:807-810.

Markram H, Helm PJ, Sakmann B (1995) Dendritic calcium transients evoked by single back-propagating action potentials in rat neocortical pyramidal neurons. J Physiol 485 (Pt 1):1-20.

Markram H, Lubke J, Frotscher M, Sakmann B (1997) Regulation of synaptic efficacy by coincidence of postsynaptic APs and EPSPs. Science 275:213-215.

Markram H, Lubke J, Frotscher M, Roth A, Sakmann B (1997) Physiology and anatomy of synaptic connections between thick tufted pyramidal neurones in the developing rat neocortex. J Physiol 500 (Pt 2):409-440.

Midtgaard J (1992) Membrane properties and synaptic responses of Golgi cells and stellate cells in the turtle cerebellum in vitro. J Physiol 457:329-354.

Misgeld U, Bijak M, Jarolimek W (1995) A physiological role for GABAB receptors and the effects of baclofen in the mammalian central nervous system. Prog Neurobiol 46:423-462.

Neher E, Sakmann B (1976) Single-channel currents recorded from membrane of denervated frog muscle fibres. Nature 260:799-802.

Nicoll RA, Malenka RC (1995) Contrasting properties of two forms of long-term potentiation in the hippocampus. Nature 377:115-118.

Numberger M, Draguhn A (1996) Patch-Clamp-Technik. Spektrum Akademischer Verlag.

Oheim M, Beaurepaire E, Chaigneau E, Mertz J, Charpak S (2001) Two-photon microscopy in brain tissue: parameters influencing the imaging depth. J Neurosci Methods 111:29-37.

Palay S, Chan-Palay V (1974) Cerebellar Cortex. Cytoloy and Organization. Springer Verlag.

Pouzat C, Marty A (1999) Somatic recording of GABAergic autoreceptor current in cerebellar stellate and basket cells. J Neurosci 19:1675-1690.

Rahamimoff R (1968) A dual effect of calcium ions on neuromuscular facilitation. J Physiol 195:471-480.

Redman S (1990) Quantal analysis of synaptic potentials in neurons of the central nervous system. Physiol Rev 70:165-198.

Reyes A, Lujan R, Rozov A, Burnashev N, Somogyi P, Sakmann B (1998) Target-cell-specific facilitation and depression in neocortical circuits. Nat Neurosci 1:279-285.

Rivera C, Voipio J, Payne JA, Ruusuvuori E, Lahtinen H, Lamsa K, Pirvola U, Saarma M, Kaila K (1999) The K+/Cl- co-transporter KCC2 renders GABA hyperpolarizing during neuronal maturation. Nature 397:251-255.

Rossi DJ, Hamann M (1998) Spillover-mediated transmission at inhibitory synapses promoted by high

affinity alpha6 subunit GABA(A) receptors and glomerular geometry. Neuron 20:783-795.

Rusakov DA, Saitow F, Lehre KP, Konishi S (2005) Modulation of presynaptic Ca^{2+} entry by AMPA receptors at individual GABAergic synapses in the cerebellum. J Neurosci 25:4930-4940.

Satake S, Saitow F, Yamada J, Konishi S (2000) Synaptic activation of AMPA receptors inhibits GABA release from cerebellar interneurons. Nat Neurosci 3:551-558.

Satake S, Saitow F, Rusakov D, Konishi S (2004) AMPA receptor-mediated presynaptic inhibition at cerebellar GABAergic synapses: a characterization of molecular mechanisms. Eur J Neurosci 19:2464-2474.

Satake S, Song SY, Cao Q, Satoh H, Rusakov DA, Yanagawa Y, Ling EA, Imoto K, Konishi S (2006) Characterization of AMPA receptors targeted by the climbing fiber transmitter mediating presynaptic inhibition of GABAergic transmission at cerebellar interneuron-Purkinje cell synapses. J Neurosci 26:2278-2289.

Schenk U, Verderio C, Benfenati F, Matteoli M (2003) Regulated delivery of AMPA receptor subunits to the presynaptic membrane. Embo J 22:558-568.

Schiller J, Helmchen F, Sakmann B (1995) Spatial profile of dendritic calcium transients evoked by action potentials in rat neocortical pyramidal neurones. J Physiol 487 (Pt 3):583-600.

Sigworth FJ, Affolter H, Neher E (1995) Design of the EPC-9, a computer-controlled patch-clamp amplifier. 2. Software. J Neurosci Methods 56:203-215.

Silver RA, Cull-Candy SG, Takahashi T (1996) Non-NMDA glutamate receptor occupancy and open probability at a rat cerebellar synapse with single and multiple release sites. J Physiol 494 (Pt 1):231-250.

Smith SL, Otis TS (2005) Pattern-dependent, simultaneous plasticity differentially transforms the input-output relationship of a feedforward circuit. Proc Natl Acad Sci U S A 102:14901-14906.

Soler-Llavina GJ, Sabatini BL (2006) Synapse-specific plasticity and compartmentalized signaling in cerebellar stellate cells. Nat Neurosci 9:798-806.

Spence DE, Kean PN, Sibbett W (1991) 60-fsec pulse generation from a self mode-locked Ti:sapphire laser. Optics Communications 104:223.

Stevens CF, Wang Y (1995) Facilitation and depression at single central synapses. Neuron 14:795-802.

Stuart GJ, Sakmann B (1994) Active propagation of somatic action potentials into neocortical pyramidal cell dendrites. Nature 367:69-72.

Stuart GJ, Dodt HU, Sakmann B (1993) Patch-clamp recordings from the soma and dendrites of neurons in brain slices using infrared video microscopy. Pflugers Arch 423:511-518.

Svoboda K, Block SM (1994) Biological applications of optical forces. Annu Rev Biophys Biomol Struct 23:247-285.

Svoboda K, Yasuda R (2006) Principles of two-photon excitation microscopy and its applications to neuroscience. Neuron 50:823-839.

Takago H, Nakamura Y, Takahashi T (2005) G protein-dependent presynaptic inhibition mediated by

AMPA receptors at the calyx of Held. Proc Natl Acad Sci U S A 102:7368-7373.

Takayama C, Inoue Y (2005) Developmental expression of GABA transporter-1 and 3 during formation of the GABAergic synapses in the mouse cerebellar cortex. Brain Res Dev Brain Res 158:41-49.

Thomson AM, Deuchars J, West DC (1993) Single axon excitatory postsynaptic potentials in neocortical interneurons exhibit pronounced paired pulse facilitation. In: Neuroscience, pp 347-360.

Tsou K, Nogueron MI, Muthian S, Sanudo-Pena MC, Hillard CJ, Deutsch DG, Walker JM (1998) Fatty acid amide hydrolase is located preferentially in large neurons in the rat central nervous system as revealed by immunohistochemistry. Neurosci Lett 254:137-140.

Vardi N, Zhang LL, Payne JA, Sterling P (2000) Evidence that different cation chloride cotransporters in retinal neurons allow opposite responses to GABA. J Neurosci 20:7657-7663.

Wahl LM, Stratford KJ, Larkman AU, Jack JJ (1995) The variance of successive peaks in synaptic amplitude histograms: effects of inter-site differences in quantal size. Proc Biol Sci 262:77-85.

Wang Y, Small DL, Stanimirovic DB, Morley P, Durkin JP (1997) AMPA receptor-mediated regulation of a G_i-protein in cortical neurons. Nature 389:502-504.

Wilson T, Sheppard C (1984) Theory and Practice of Scanning Optical Microscopy (New York; Acedemic Press).

Yamada M, Inanobe A, Kurachi Y (1998) G protein regulation of potassium ion channels. Pharmacol Rev 50:723-760.

Yaroslavsky AN, Schulze PC, Yaroslavsky IV, Schober R, Ulrich F, Schwarzmaier HJ (2002) Optical properties of selected native and coagulated human brain tissues in vitro in the visible and near infrared spectral range. Phys Med Biol 47:2059-2073.

Yuste R, Denk W (1995) Dendritic spines as basic functional units of neuronal integration. Nature 375:682-684.

Zipfel WR, Williams RM, Webb WW (2003) Nonlinear magic: multiphoton microscopy in the biosciences. Nat Biotechnol 21:1369-1377.

Zucker RS (1989) Short-term synaptic plasticity. Annu Rev Neurosci 12:13-31.

7. ABSTRACTS

Astori S, Köhr G (2005) Presynaptic AMPA receptors modulate GABA release in cerebellar stellate cells. Washington DC, Society for Neuroscience.

Meyer S, Yang Y, Astori S, Zhu P, Migala A, Nagai T, Miyawaki A, Mank M, Griesbeck O, Palmer AE, Tsien RY, Nakai J, Denk W, Sprengel R, Hasan MT (2006) Functional fluorescent calcium indicator proteins targeted to neurons using adeno-associated viral expression systems. Atlanta, Society for Neuroscience.

8. ACKNOWLEDGEMENTS

I want to thank everyone who supported me during my PhD:

PD Dr. Georg Köhr for giving me the opportunity to enrich my theoretical background by introducing me into the experimental research in a new field.

Prof. Dr. Peter H. Seeburg for the excellent working conditions in the Department of Molecular Neurobiology of MPI.

Prof. Dr. Josef Bille for his interest in my project and for supervision in the Faculty for Physics.

Dr. Bettina Schupp for helpful assistance during the first years of my PhD and continuous encouragement.

Dr. Verena Pawlak for friendly support and correction of the thesis.

Sven Berberich, Pradeep Punnakkal and all colleagues from the Department of Molecular Neurobiology for the nice working and social atmosphere.

Dr. Beril Doganci for friendly support.

Dr. Günter Giese for technical advice in 2P microscopy.

Prof. Dr. Thomas Kuner for the Minis Analysis Macro.

Prof. Egidio D'Angelo and his collaborators in Pavia for guiding my very first steps in the electrophysiology.

Peter Brandt and his family for making my stay in Heidelberg more pleasant.

My family for continuous support.